

**NOVEL EXPANDED TITANATE BASED MATERIALS FOR ENERGY  
APPLICATIONS**

by

**MIAD YARALI**

Submitted to the Graduate School of Engineering and Natural Science

in partial fulfillment of

the requirements for the degree of

Master of Science

Sabanci University

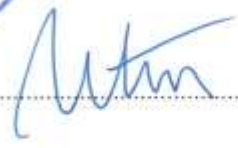
July 2015

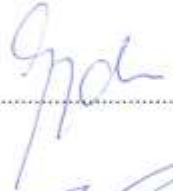
Novel expanded titanate based materials for energy applications

APPROVED BY:

Assoc. Prof. Dr. Selmiye Alkan Gürsel (Thesis Supervisor) 

Dr. Alp Yürüm (Thesis co-advisor) 

Assist.Prof. Dr. Oktay Demircan 

Assist. Prof. Dr. Gözde İnce 

Assist. Prof. Dr. Fevzi Ç. Cebeci 

DATE OF APPROVAL: 29/07/2015

©Miad Yarali 2015

All Rights Reserved

NOVEL EXPANDED TITANATE BASED MATERIALS FOR ENERGY  
APPLICATIONS

MIAD YARALI

MAT, M.Sc. Thesis, 2015

Thesis Supervisor: Assoc. Prof. Dr. Selmiye Alkan Gürsel

Co-Supervisor: Dr. Alp Yürüm

**Keywords:** Titanate nanotubes, Hydrothermal Treatment, Li-ion, Anode, Electrochemical Performance

**ABSTRACT**

Development of lithium-ion batteries operating at high charge and discharge rates is highly demanded especially for electronic devices and electric vehicles. For this purpose, improvement of ion transport in the crystal structure is needed. In this respect, the general strategy is reducing down the particle size to a nanometer scale. This helps to decrease the ion diffusion length. Titanate nanotubes are promising materials because of their special morphology and high specific surface area. These titanates provide high rate capability and low volume expansion upon lithiation. More importantly their tubular structure helps the transport of ions through the crystal. In this study, we synthesized titanate nanotubes

hydrothermally from commercial and sol-gel TiO<sub>2</sub>. Moreover, the interlayer distances of the nanotubes were modified by changing the pH and the addition of surfactants.

For the characterization, SEM, XRD, BET and TEM techniques were used. In addition, the effect of interlayer distance on energy capacity and rate capability was investigated. The shortest interlayer distance was observed at pH value of 4.4. Getting further away from this point, interlayer distances increased and this also increased the nanotube diameter. Conversely, specific surface area reaches its maximum value of 334 m<sup>2</sup>/g at pH of 4.4. Potential-capacity profiles of TiO<sub>2</sub> (anatase) nanoparticles showed distinct potential plateaus at 1.7 and 2.2 V for discharging and charging, respectively. However, the capacity dropped from 254 mAh/g to 87 mAh/g in 10 cycles. For titanates, broad peaks appear in CV measurement, thus no distinct plateau was observed at potential-capacity profile. For titanates before surfactant treatment capacities as high as 980 mAh/g were obtained. After surfactant treatment the capacity reached to 1232 mAh/g. More importantly, titanates showed exceptional rate capabilities especially at wider interlayer distances due to higher mobility of ions in the structure. It was found that interlayer distance plays an important role in rate capability. In addition, we achieved significant expansion in interlayer distances after post-treatment with the surfactants which can enhance the ion mobility.

ENERJİ UYGULAMALARI İÇİN GENİŞLETİLMİŞ TİTANAT ESASLI  
YENİ MALZEMELER

MIAD YARALI

MAT, M.Sc. Tezi, 2015

Tez Danışmanı: Doç. Dr. Selmiye Alkan Gürsel

Ortak Tez Danışmanı: Dr. Alp Yürüm

**Anahtar Kelimeler:** Titanat nanotüpler, Hidrotermal İşlem, Li-iyon, Anot,  
Elektrokimyasal Performans

**ÖZET**

Elektronik cihazlarda ve araçlarda kullanılabilir yüksek şarj ve deşarj oranlarında çalışabilen lityum-iyon bataryalarının geliştirilmesi oldukça önemli bir gereklilik haline gelmiştir. Bu amaçla, batarya içinde kristal yapıdaki iyon hareketini iyileştirmek gerekmektedir. Bu bağlamda uygulanan genel strateji ise parçacık boyutunu nanometer skalasına düşürmek olmaktadır. Bu sayede iyon difüzyon uzunluğunun düşürülmesine yardımcı olmaktadır. Titanat nanotüpler, özel morfolojileri ve yüksek yüzey alanları

sayesinde umut vadecici malzemelerdir. Bu titanatların lityumun tepkimesi sırasında yüksek hız kapasitesi ve düşük hacim genişlemesi sağlamaları da beklenmektedir. Ayrıca, bu titanat nanotüplerin boru şeklindeki yapıları sayesinde iyonların kristale taşınmalarını da kolaylaştıracağı düşünülmüştür.

Bu çalışmada, titanat nanotüplerinin, ticari ve sol-jel  $TiO_2$ 'den başlanarak hidrotermal yöntemle sentezleri başarıyla gerçekleştirilmiştir. Ardından, nanotüpler arasındaki tabakaların açılması için değişen pH'larda çalışılıp pH etkisi incelenmiş ve ayrıca surfactant eklenerek bu etki de araştırılmıştır.

Elde edilen yapıların detaylı karakterizasyonları için SEM, XRD, BET ve TEM teknikleri kullanılmıştır. Özellikle, tabakalar arası uzaklığın enerji kapasitesi ve hız kapasitesine etkisi araştırılmıştır.  $pH=4.4$ 'da tabakalar arasındaki en düşük uzaklık elde edilmiştir. Bu değerden sonra tabakalar arası uzaklık artırmış ve nanotüplerin çapları da artmıştır. Ayrıca,  $pH= 4.4$ 'da özgül yüzey alanının maksimum değere ulaştığı ve  $334 \text{ m}^2/\text{g}$  olduğu saptanmıştır.  $TiO_2$  (anataz) nanoparçacıklarının potansiyel- kapasite profilleri çıkarıldığında,  $1.7 \text{ V}$  değerinde deşarj ve  $2.2 \text{ V}$  değerinde şarj için plato değerleri gözlemlenmiştir. Kapasite değerinin 10 çevrim sonrasında  $254 \text{ mAh/g}$  'den  $87 \text{ mAh/g}$ 'e düştüğü görülmüştür. Titanatlar için gerçekleştirilen CV ölçümlerinde ise geniş pikler elde edilmiş ayrıca belirgin bir plato değeri gözlemlenmemiştir. Yüzey aktif madde ile işleminden önce titanatlar için oldukça yüksek bir kapasite değeri,  $980 \text{ mAh/g}$ , elde edilmiştir. Yüzey aktif madde ile işlemden sonra ise kapasite  $1232 \text{ mAh/g}$  değerine ulaşmıştır. Daha önemlisi, tabakalar arası genişletilmiş titanatlar için oldukça yüksek hız kapasiteleri elde edilmiştir. Tabakalar arası uzaklığın kapasite için oldukça önemli olduğu sonucuna varılmıştır. Ayrıca surfactant sayesinde tabakaların açıldığı ve iyon hareketinin artırıldığı da gösterilmiştir.



*To my lovely family*

## ACKNOWLEDGEMENT

Firstly, I would like to express my sincere gratitude to my thesis advisor Assoc. Prof. Dr. Selmiye Alkan Gürsel not only for her continuous support of my MSc study but also for her patience, motivation and comprehensive knowledge. During this period she has never stopped devoting her time and resources to improve my work. I hope that one day I would become as helpful a professor to my students as Dr. Gürsel has been to me.

Secondly, I want to mention my deeply appreciation to my co-advisor, Dr. Alp Yürüm whose constructive comments and guidance have always been of tremendous help to pave my way through success. His academic and personal pieces of advice has been helping me in all the time of research and writing of this thesis. I could not have imagined having a better co-advisor and mentor for my MSc study as I had the best by my side.

Thirdly, I would like to thank Dr. Emre Biçer for his support and guidance as well throughout this study.

I would like to thank my thesis defense jury that has honored me to by accepting to be members of my defense jury.

Furthermore, I want to thank all of my friends in Sabanci University. Many friends have helped me stay sane through these difficult years. Their support and kind care helped me overcome setbacks and stay meticulously focused on my graduate study. I greatly value their friendship and I deeply appreciate their belief in me.

Most importantly, none of this would have been possible without the love and patience of my family. My immediate family, to whom this dissertation is dedicated to, has been a constant source of love, concern, support and strength all these years. I would like to express my heart-felt appreciation and warmest regards to my family.

## Table of contents

<b>ABSTRACT</b> .....	<b>IV</b>
<b>ÖZET</b> .....	<b>VI</b>
<b>ACKNOWLEDGEMENT</b> .....	<b>X</b>
<b>LIST OF FIGURES</b> .....	<b>XIII</b>
<b>LIST OF TABLES</b> .....	<b>XV</b>
<b>1. INTRODUCTION</b> .....	<b>1</b>
<b>1.1. Common secondary battery types</b> .....	<b>1</b>
<b>1.2. Lithium ion batteries</b> .....	<b>3</b>
<b>1.3. Cathode materials</b> .....	<b>7</b>
<b>1.4. Anode materials</b> .....	<b>8</b>
1.4.1. Titanium dioxide (TiO <sub>2</sub> ) as the anode.....	12
1.4.2. Sol-gel method .....	22
1.4.3. Hydrothermal Treatment .....	24
1.4.4. Surfactant treatment.....	27
<b>1.5. Objectives</b> .....	<b>28</b>
<b>2. MATERIALS AND METHODS</b> .....	<b>29</b>
<b>2.1. Sol-gel synthesis</b> .....	<b>29</b>
<b>2.2. Hydrothermal treatment</b> .....	<b>30</b>
<b>2.3. Surfactant treatment</b> .....	<b>32</b>
<b>2.4. Structural characterization</b> .....	<b>32</b>
<b>2.5. Electrochemical characterization studies</b> .....	<b>33</b>
<b>3. RESULTS AND DISCUSSION</b> .....	<b>36</b>

<b>3.1. Structural and electrochemical properties of TiO<sub>2</sub> samples.....</b>	<b>36</b>
3.1.1. Thermal characterization.....	36
3.1.2. XRD characterization .....	37
3.1.3. SEM characterization.....	38
3.1.4. Surface area and pore size analyses.....	39
3.1.5. Electrochemical characterization.....	40
<b>3.2. Structural and electrochemical properties for titanate samples .....</b>	<b>43</b>
3.2.1. XRD characterization .....	44
3.2.2. SEM characterization.....	45
3.2.3. Surface area and pore size analyses.....	47
3.2.4. Electrochemical characterization.....	48
<b>3.3. Structural characterization of surfactant treated titanates .....</b>	<b>51</b>
3.3.1. XRD characterization .....	52
3.3.2. SEM and TEM characterization .....	53
3.3.3. Surface area and pore size analyses.....	55
3.3.4. Electrochemical characterization.....	56
<b>4. CONCLUSION.....</b>	<b>58</b>
<b>REFERENCES.....</b>	<b>59</b>

## List of Figures

Figure 1. Secondary batteries comparison of energy density .....	3
Figure 2. Schematic assembly of a LIB using lithium cobalt oxide ( $\text{LiCoO}_2$ ) as cathode and graphite as anode.....	4
Figure 3. Voltage-capacity profile of $\text{Li}_x(\text{Ni}_{1/3}\text{Co}_{1/3}\text{Mn}_{1/3}\text{O}_2)$ cathode as an example of a typical voltage-capacity pattern .....	6
Figure 4. Typical cyclic voltammetry profile .....	6
Figure 5. Three main groups of materials, which are used in LIBs and their properties and schematic drawn mechanism. Yellow circles: lithium ions, black circles: pores in crystal structure, blue circles: metal atoms .....	9
Figure 6. Dendrite process.....	11
Figure 7. (a) location of Ti and O atoms in unit cell of anatase, (b) bonds between Ti and O atoms, (c) location of each Ti and O atoms .....	14
Figure 8. Anatase phase structure of $\text{TiO}_2$ .....	15
Figure 9. Rutile phase structure of $\text{TiO}_2$ .....	16
Figure 10. Brookite phase structure of $\text{TiO}_2$ .....	17
Figure 11. $\text{TiO}_2$ (B) phase structure of $\text{TiO}_2$ .....	18
Figure 12. Scroll shape of titanate nanotube.....	19
Figure 13. $\text{Li}^+$ intercalated zig-zag layers structure of titanate with $\text{Li}^+$ , $\text{H}^+$ and $\text{Na}^+$ between its layers.....	20
Figure 14. Schematic presentation of sol-gel process .....	23
Figure 15. Schematic formation mechanism of titanate nanotubes .....	25
Figure 16. Protherm calcination furnace .....	29
Figure 17. Schematic mechanism of sol-gel method .....	30
Figure 18. Teflon-lined autoclave .....	31
Figure 19. Schematic mechanism of hydrothermal treatment .....	31
Figure 20. Schematic mechanism of surfactant treatment.....	32
Figure 21. a) Copper foil, b) coated copper foil, c) lithium chip and d) separator .....	33
Figure 22. Assembled lithium-ion battery.....	34
Figure 23. Preparation of anode.....	34
Figure 24. TGA/DTA curves of SG .....	37

Figure 25. XRD diffraction patterns of Com and SG .....	38
Figure 26. SEM images of a) Com, and b) SG .....	39
Figure 27. Pore size distributions of Com and SG using BJH method .....	40
Figure 28. Cyclic voltammetry of Com and SG .....	41
Figure 29. First three charge-discharge curves at 0.1C for a) Com, and b) SG and evolution of reversible capacity at different current rates over 20 cycles for c) Com, and d) SG .....	42
Figure 30. Rate capabilities of Com and SG .....	43
Figure 31. XRD patterns of titanates samples washed in solutions with different pH values. (a) NC, (b) NS.....	45
Figure 32. SEM images of NC samples with pH values of (a) 4, (b) 7.2, (c) 9.8 and (d) 1146	
Figure 33. SEM images of NS samples with pH values of (a) 2.4, (b) 3.3, (c) 5.2, (d) 6.5 and (e) 13 .....	47
Figure 34. (a, b) NC samples a) surface area, b) interlayer distances, (c, d) NS samples c) surface area, d) interlayer distance .....	48
Figure 35. Cyclic voltammetry of a) NC4, and b) NC9.8 .....	49
Figure 36. First three charge-discharge curves at 0.1C for NC samples washed in pH value of a) 4, and b) 9.8, and evolution of reversible capacity at different current rates in 20 cycles for c) NC4, and d) NC9.8.....	50
Figure 37. Rate capabilities of a) NC4, and b) NC9.8 .....	51
Figure 38. Comparison between XRD patterns of a) NC and SNC samples, and b) NS and SNS samples .....	53
Figure 39. SEM images of a) NC4, b) SNC4, c) NS5.2, and d) SNS5.2 .....	54
Figure 40. TEM images of NC4.4 and SNC4.4 .....	54
Figure 41. Comparison of a) surface area of NC and SNC samples, b) interlayer distances of NC and SNC samples, c) surface area of NS and SNS samples and d) interlayer distances of NS and SNS samples.....	56
Figure 42. Discharge capacity of a) NC4.4, and b) SNC4.4 at 0.1C in 19 cycles .....	57

## List of Tables

Table 1. Structural parameters of titanium dioxide polymorphs .....	12
Table 2. Main XRD peaks of anatase, rutile and brookite phases .....	13
Table 3. Electrochemical properties of hydrothermal treated TiO <sub>2</sub> .....	21
Table 4. H <sub>2</sub> Ti <sub>3</sub> O <sub>7</sub> nanotubes prepared by different TiO <sub>2</sub> precursors, experimental and post-treatment conditions .....	26

## 1. Introduction

Energy is the most important issue that all countries around the world are concerned about. Due to their high energy densities and relatively lower costs, mainly fossil fuels are preferred for energy generation. Fossil fuels were significantly consumed within the last 100 years due to increase in the world population and consequently resulted in high energy demand [1]. It is known that consumption of fossil fuels has resulted in mass production of green house gasses and by-products. As a consequence air pollution has become a major issue all around the world thus some new technologies such as nuclear and renewable energy were considered as alternatives in the last decades. The former, however has its problems like nuclear waste and low safety, therefore most of the attention is on the renewable sources of energy such as wind and solar power as well as environment friendly fuels [2]. For that reason, we need to use more renewable energy resources and decrease our reliance on fossil fuels. More importantly, due to our high energy need, we need easily acquired sources of energy that satisfy our energy demand whenever it is needed. Today, even after decades of improvement in renewable energy systems, 95% of the energy in the world is still provided by fossil fuels, nuclear power and traditional hydropower. The missing thing from the present picture that could dramatically increase the use of renewable energy is improved energy storage. Storage breaks out into two domains. First, is portable storage, specifically batteries, the kind that we use in our laptops and mobile phones which requires relatively lower energy densities and current rates. The second one which is more important is storage for applications like electric cars and grid scale power storage. Electric vehicles and grid storage devices have potential to become feasible alternatives to current technology, if we can improve energy storage materials for Li-ion batteries that offer high capacity and high rate capabilities [3].

### 1.1. Common secondary battery types

Secondary batteries (rechargeable) can be found anywhere around us and our world is highly influenced by them. They provide the opportunity to charge an empty battery and use them again therefore they are financially beneficial.

Lead- Acid Batteries: These batteries are made of two lead plates as electrodes. They are considered as the oldest types of secondary batteries. They provide low specific energy and also less cycle life. They are commonly used in emergency lighting and drain applications.

Nickel- Cadmium Batteries (Ni-Cd): It can be implied from its name that this type of battery is made of two electrodes based on nickel and cadmium. They are used when high discharge current is needed. They can also operate at high temperatures and their main application is power tools.

Nickel-Metal-Hydride Batteries (Ni-MH): They contain two electrodes based of Nickel and a metal hydride, the common metal hydride which is used as an electrode in this type of batteries is Lanthanum (La) [4]. They can provide a high energy density (800 Wh/kg) and they are able to reserve energy density even at high current rates [5]. They are generally used in hybrid cars.

Lithium ion Batteries (LIBs<sup>1</sup>): LIBs compared to other battery types have some benefits such as less weight, high energy density, almost zero self-discharge and no memory effect which make LIBs as the promising electrical energy storage device for modern portable electronic applications [6, 7]. This convinced the global markets to do investments on LIBs and increase the amount of mass production of LIBs over the past years. Moreover it was forecasted that volume of sales will be raised to 20 billion dollar in 2020 [8].

---

<sup>1</sup> Lithium ion batteries

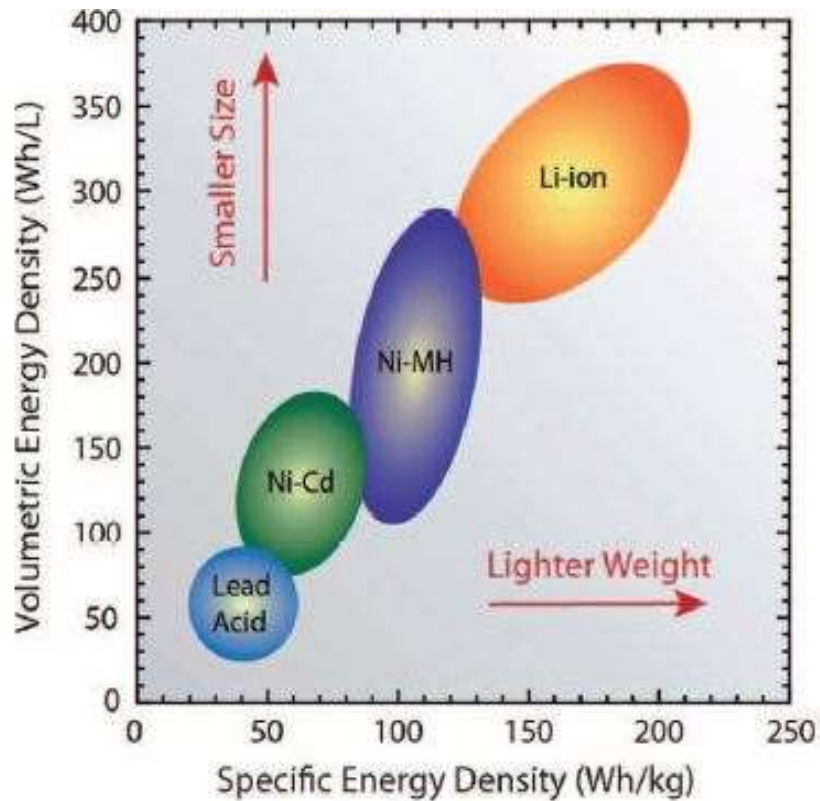


Figure 1. Secondary batteries comparison of energy density [9]

## 1.2. Lithium ion batteries

Like the other secondary batteries, LIBs are made of several compressed cells. Any cell contains two electrodes as an anode and cathode, a chemical component known as electrolyte is between them, and two current collectors which are typically copper and aluminum that are connected to anode and cathode, respectively. If the electrolyte is liquid, a separator is used in order to keep the electrodes apart from each other, but if the electrolyte is solid, there is no need for a separator. Schematic drawing of a typical lithium ion battery is shown in Fig.2. Almost 35 years ago the first LIB presented and the anode was graphite and lithium cobalt oxide ( $\text{LiCoO}_2$ ) was used as cathode [10]. Charge - discharge processes are the results of  $\text{Li}^+$  migration between anode and cathode. During charging, the  $\text{LiCoO}_2$  structure, which stores  $\text{Li}^+$ , is oxidized till reaching  $\text{Li}_{0.5}\text{CoO}_2$  (equation 1) and  $\text{Li}^+$  ions moves toward anode through an ion conductive electrolyte and

inserted into graphite lattice which is reducing it to  $\text{LiC}_6$  (equation 2). In order to get electrical work, two current collectors are connected to each other and make an external circuit; electrons can be easily conducted throughout this circuit. Discharge is the reverse process of charging; the lithium ions are transferred from cathode and inserted to graphite lattice and reverse reactions happen in both electrodes resulting in a potential of about 3.9 V. Equation 1 and 2 show the reactions in cathode and anode, respectively [3].

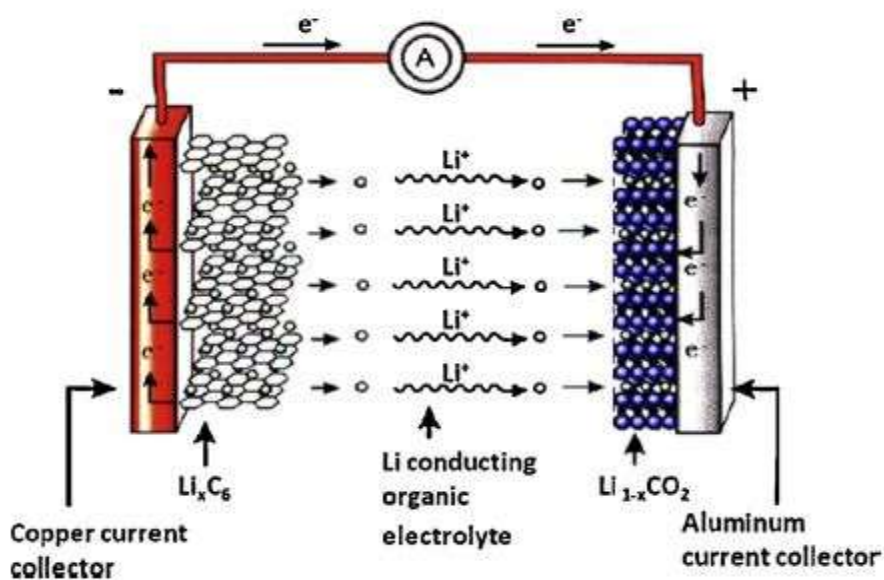
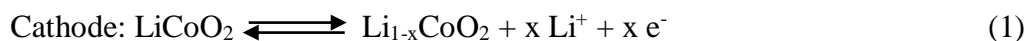


Figure 2. Schematic assembly of a LIB using lithium cobalt oxide ( $\text{LiCoO}_2$ ) as cathode and graphite as anode [3]



Each material has its specific reduction and oxidation potential indicating that when the materials are used in a cell, their potential differences would give the overall potential of that cell (equation 4).

$$E^{\circ}_{\text{cell}} = E^{\circ}_{\text{cathode}} - E^{\circ}_{\text{anode}} \quad (4)$$

Theoretical capacity of the battery can be calculated by using the following equation where  $q$  is the theoretical capacity (mAh/g),  $n$  is the number of electrons transferred,  $F$  is the Faraday constant (As/mole) and  $M$  is the molar mass (kg/mole) of the host material [11].

$$q = \frac{nF}{3600 \times M} \quad (5)$$

For instance, if  $\text{LiFePO}_4$  is used as cathode, its theoretical capacity can be calculated by equation 5.



Here  $n=1$  and molar mass of  $\text{LiFePO}_4$  is  $157.7 \times 10^{-3}$  kg/mole and faraday constant is 96500 As/mole. By using equation 5, the capacity would be 170 mAh/g.

Practical specific capacity is the amount of capacity that battery delivers in a determined cutoff potential at constant current rate. This capacity can be calculated by the following equation [11].

$$\text{Practical specific capacity} = \frac{i \times A \times t}{3600 \times W} \quad (6)$$

In this equation  $i$  ( $\text{A/m}^2$ ) is the current rate,  $A$  ( $\text{m}^2$ ) is the area of electrode,  $t$  (second) is the duration of battery working till reaching cutoff potential and  $W$  (kg) is the weight of the active material. Fig. 3 shows voltage-capacity of  $\text{Li}_x(\text{Ni}_{1/3}\text{Co}_{1/3}\text{Mn}_{1/3})\text{O}_2$  cathode at C/30 current rate as an example of a typical voltage-capacity profile. The capacity axis is calculated by equation 6. As it can be seen the practical capacity of this material is 165 mAh/g which is less than its theoretical capacity (277.8 mAh/g) [11] due to formation of  $\text{Li}_x(\text{Ni}_{1/3}\text{Co}_{1/3}\text{Mn}_{1/3})\text{O}_2$  where  $x$  cannot reach to its maximum value of 1.

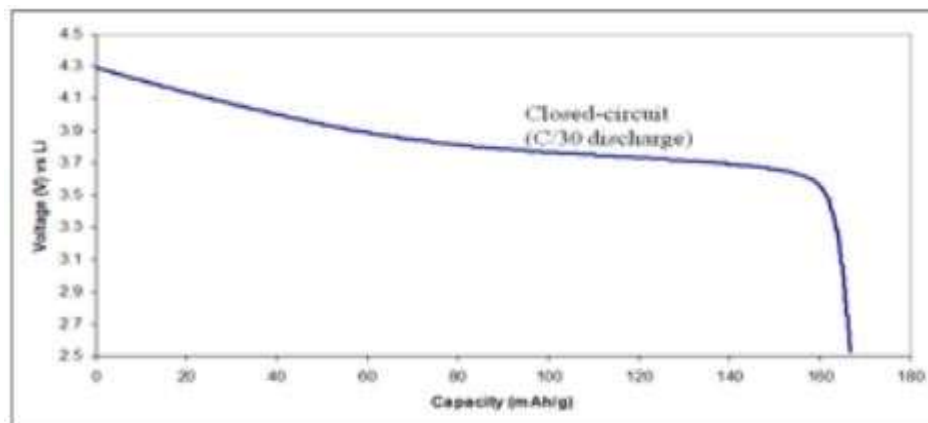


Figure 3. Voltage-capacity profile of  $\text{Li}_x(\text{Ni}_{1/3}\text{Co}_{1/3}\text{Mn}_{1/3}\text{O}_2)$  cathode as an example of a typical voltage-capacity pattern [11]

Furthermore oxidation–reduction voltages are studied with cyclic voltammetry (CV) technique where the voltage of electrode is scanned with respect to current from an initial value to a determined limit. When the voltage reaches to the up limited value, the direction of the scan is reversed. By utilizing this technique, we are able to know in which voltage oxidation and reduction occur. It has generally two peaks corresponding to oxidation and reduction. Fig. 4 represents a typical CV curve.

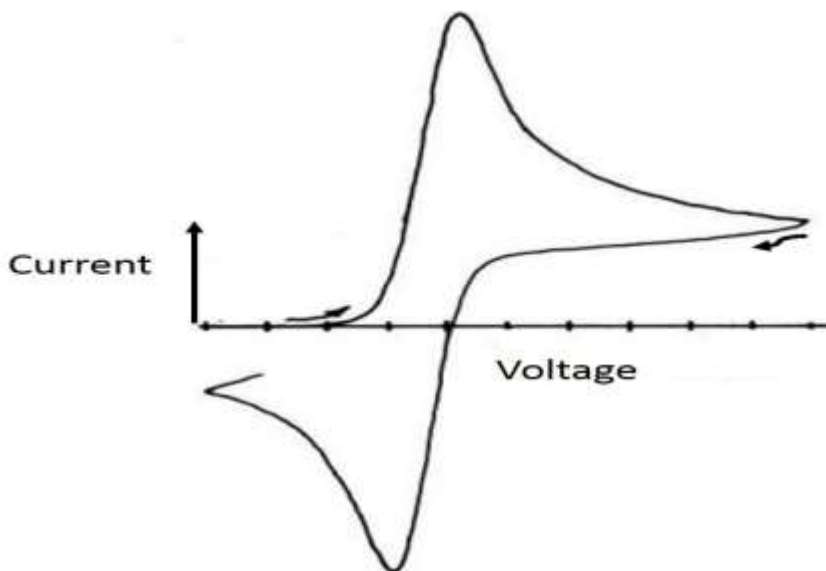


Figure 4. Typical cyclic voltammetry profile

Unlike other batteries, LIBs can be assembled using different materials to make the anode and cathode to store more lithium ions.

### 1.3. Cathode materials

One of the most important factors to choose a high performance cathode material is its structure. Most cathode materials have the layered structure of  $\alpha$ -NaFeO<sub>2</sub>, which provides more mobility for Li<sup>+</sup>. Cathode materials are generally categorized in three types.

The first type is lithium metal oxide like layered structure LiCoO<sub>2</sub>. It has high discharge voltage (4.2 V) associated with specific energy of 590 Wh/kg and specific charge of 140 Ah/kg [12]. Utilizing this material as cathode has some disadvantages. Its high discharge potential may decompose the electrolyte and leads to decreasing of the battery performance [12]. Its cycle performance is not adequate for some applications like electric vehicles also capacity fading was reported for LiCoO<sub>2</sub> as cathode material [13].

The second type of cathode materials is transition metal phosphates like LiFePO<sub>4</sub> (LFP). LFP can be a standard candidate for cathode material in high power density LIBs because of its high capacity, excellent cycling performance and low cost. Its main advantage is high specific power up to 1500 W/kg also its discharge potential, specific capacity and specific energy is 3.4 V, 170 Ah/kg and 580 Wh/kg, respectively [14]. Poor electronic conductivity as well as low Li<sup>+</sup> diffusion rate can be considered as the major disadvantages of LFP as a cathode material.

The third type of cathode material is spinel type. LiMn<sub>2</sub>O<sub>4</sub> is well-known material in this type. It was reported that carbon coated LiMn<sub>2</sub>O<sub>4</sub> cathode has excellent rate capability [15]. Capacity fading as the result of Mn<sup>2+</sup> insertion into electrolyte and low specific capacity (300 Wh/kg) are the main disadvantages of LiMn<sub>2</sub>O<sub>4</sub> [16]

#### 1.4. Anode materials

Anode in LIBs is generally fabricated from three main groups, alloying, conversion and intercalation type materials. The first group can easily make several steps of alloying with  $\text{Li}^+$  to come up with  $\text{Li}_x\text{A}$  ( $\text{A} = \text{Ge}, \text{Si}, \text{SiO}, \text{Sn}, \text{SnO}_2$ , etc). They have high theoretic capacity in the range of 783 mAh/g for  $\text{SnO}_2$  to 4211 mAh/g for Si. These materials are not used as anode electrode due to their great volumetric increase when they combine with lithium [3]. Huge efforts have been done to control volume change like trying to buffer the unstable volume by blending with appropriate additives but still they did not meet the life range, safety and cycle stability requirements [17]. In the case of Si which has the highest theoretical capacity among alloying materials, several lithium rich phases form ( $\text{Li}_{13}\text{Si}_4$ ,  $\text{Li}_{12}\text{Si}_7$  and  $\text{Li}_{21}\text{Si}_5$ ) [18]. However, these phases are not formed and the material goes to an amorphous phase during electrochemical lithiation. Moreover, when  $\text{Li}^+$  are inserted to its lattice, Si will be expanded which significantly leads to formation of some cracks and capacity fading [18].

Conversion type materials are based on binary transition metal compounds and have the general formula  $\text{M}_a\text{X}_b$  ( $\text{M} = \text{transition metal}; \text{X} = \text{anion}$ ). When conversion type of materials react with  $\text{Li}^+$ , transition metal is fully reduced. As a result, more ions can be stored due to formation of strong crystal structure of  $\text{Li}_n\text{X}$ . However, as an important problem, they still have the high volume changes like the alloying materials [19]. Iron oxides as a conversion material have been greatly studied due to their non-toxicity and low cost. Magnetite ( $\text{Fe}_3\text{O}_4$ ) as well as hematite ( $\alpha\text{-Fe}_2\text{O}_3$ ) can reversibly react with lithium with a theoretical capacity of 926 and 1004 mAh/g, respectively [20]. Unfortunately, they have low cycling performance because of poor diffusion of  $\text{Li}^+$ , high volume change and poor electrical conductivity. However many researchers tried to modify iron oxide morphology to get better electrochemical performance [21, 22].

As a result of the mentioned drawbacks of conversion and alloying materials, the third group, intercalation materials, have been extensively tried as anode materials in LIBs but they provide less theoretical capacity than alloying and conversion materials [23]. On the

other hand, they have noticeable electrochemical properties such as long cycle life, promising cycle stability and high reversibility.

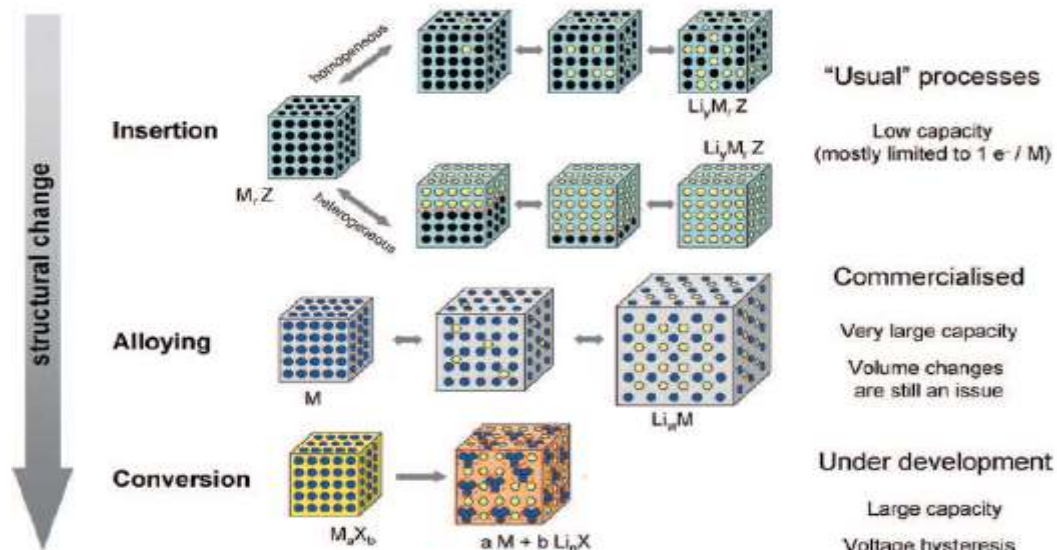


Figure 5. Three main groups of materials, which are used in LIBs and their properties and schematic drawn mechanism. Yellow circles: lithium ions, black circles: pores in crystal structure, blue circles: metal atoms [17]

Graphite as an intercalation material has high conductivity (up to  $2000 \text{ S/cm}^2$ ) due to its electronic structure. It is widely used as anode material in LIBs. It can uptake lithium ions until the formation of  $\text{LiC}_6$  where its theoretical capacity is  $372 \text{ mAh/g}$ . Multilayered graphite has the expansion of 16% when lithium ions enter its lattice (see Fig. 2). Another material that is tried anode is carbon nanotubes (CNTs) which have similar properties with graphite. Even though (single walled carbon nanotubes (SWCNTs) has the theoretical capacity up to  $1116 \text{ mAh/g}$  [24], experimentally achieving this value is a great challenge for researchers who are trying to modify morphology of SWCNTs. However a capacity in the range of  $220 - 780 \text{ mAh/g}$  was obtained [25]. Graphite based anode can reversibly place lithium ions to its multilayer structure and this can happen over thousands cycles, furthermore it has a low cost and it is abundant in environment. Moreover, lots of efforts

have been conducted on graphene [26, 27] and carbon nanofibers [28, 29] to improve the power density.

LIBs with graphite based anode electrode have low capacity (~372 mAh/g) because it allows insertion of only one  $\text{Li}^+$  with respect to six carbon atoms. This capacity is not enough for some applications that need high capacity like electric vehicles. Moreover low diffusion rate of  $\text{Li}^+$  into graphite ( $10^{-9}$ - $10^{-7}$   $\text{cm}^2/\text{s}$ ) delivers low power density [30]. Dendrite problem is another side effect of using graphite as anode. During several charge-discharge cycles of the battery, nanofibers of lithium known as dendrite are formed and they grow toward the cathode and this can cause short circuit between cathode and anode, causing it overheat and in some cases it leads to ignition (Fig. 6) [31, 32]. Another issue is the formation of solid electrolyte interphase (SEI) which is a surface film formed on anode. In most of the cases LIBs graphite anode works at -2.5 V vs. standard hydrogen electrode, and cathode which is most of the time a transition metal oxide works at +1 V thus the battery with this setup gives 3.5 V potential. This high potential makes a situation for electrolyte to be oxidized and reduced to form new substances across anode electrode [33]. Formation of SEI depends on the electrolyte type, for common electrolytes it starts to form at 2.6 V [34] This film makes electrode surface less chemically reactive with electrolyte and prevent further electrolyte decomposition.

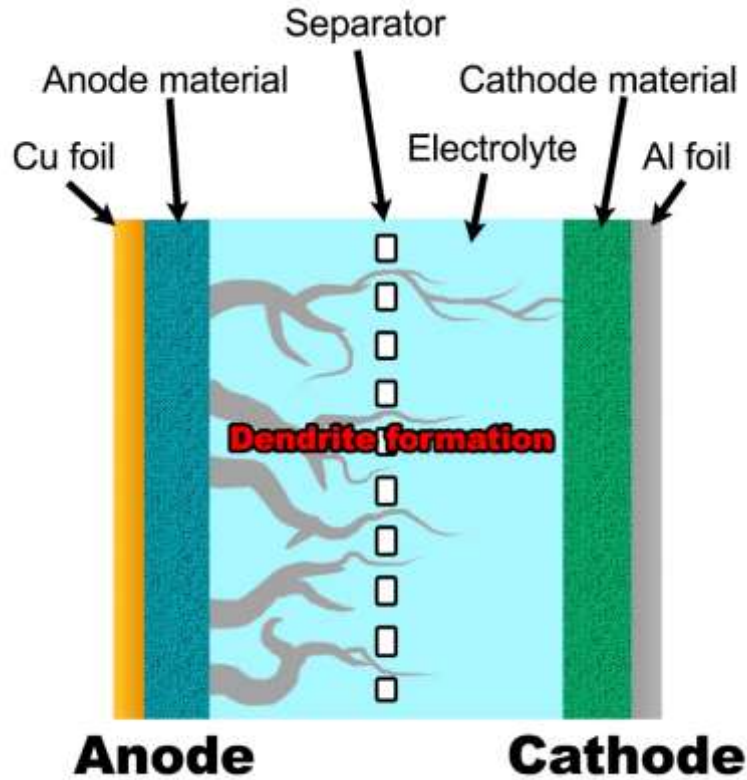


Figure 6. Dendrite process [35]

SEI film has some advantages like preventing more reactions between graphite anode with electrolyte but it also reduces power and battery's capacity because in the first charge this layer behaves like a wall and keep some lithium ions and prevent them to transfer toward cathode during discharge. In addition, during intercalation and deintercalation, due to volume volume changes some cracks may grow on the SEI layer and new SEI may form in those cracks. Over time this leads to a significant decrease in the battery's capacity [17, 36].

Many studies have been carried out to replace graphite with another active metal oxide to be used in LIBs to enhance their electrochemical performance especially the battery's capacity. Studies reveal that titanium dioxide ( $\text{TiO}_2$ ) based insertion materials can be one of the most reliable candidates to be replaced with graphite in anode of LIBs.  $\text{TiO}_2$  based anode in LIBs does not form SEI layer, six times faster charging compared to graphite and also maintain better capacity than graphite [37]. The aim of this work is modifying titanium dioxide to get higher capacity and good cycle performance.

#### 1.4.1. Titanium dioxide (TiO<sub>2</sub>) as the anode

Thanks to some noticeable properties of TiO<sub>2</sub> including low cost, environmental benignancy and non-toxicity [38], it is widely used in different applications like electronic and pigment industry, catalysis and sensors. TiO<sub>2</sub> has in different oxidation states and its cations can be easily found in environment [39]. It was reported that the state of TiO<sub>2</sub> has highly affected by the surface oxygen atoms [40].

TiO<sub>2</sub> has three main polymorphs: anatase, rutile and brookite. The first phase (anatase) is much more photoactive than the others thus it is the target materials in different industrial applications like photocatalysis, photonic crystals, electrochromics, sensors and surface coatings [41, 42]. On the other hand, the second phase (rutile), is generally used in pigments and sunscreens industry and it is the most stable phase of titanium dioxide. Brookite is not as common as anatase and rutile and it is not chemically stable just like the other polymorphs. There is also another phase of TiO<sub>2</sub> which is commonly known as TiO<sub>2</sub> (B). Table 1 shows some structural parameters of TiO<sub>2</sub> polymorphs.

Table 1. Structural parameters of titanium dioxide polymorphs [43, 44]

Structure	Density (gcm <sup>-3</sup> )	Crystal structure	Unit cell (Å)
Anatase	3.79	tetragonal	a=3.79, c=9.51
Rutile	4.13	tetragonal	a=4.59, c=2.96
Brookite	3.99	orthorhombic	a=9.17, b=5.46, c= 6.51
TiO <sub>2</sub> (B)	3.64	monoclinic	a=12.17, b=3.74, c=6.51, β=107.29°

In the crystal structure of titania, each titanium atom is coordinated with six oxygen atoms but the way this building block link to each other varies every polymorph. In all polymorphs of titania, the Ti-O length is about 2 Å and each oxygen atom is apart from each other with 2.5-3 Å distance. The main XRD peaks with their intensities are shown in Table 2.

Table 2. Main XRD peaks of anatase, rutile and brookite phases [45]

Anatase		Rutile		Brookite	
2θ (degree)	Intensity (%)	2θ (degree)	Intensity (%)	2θ (degree)	Intensity (%)
25.27	100	27.70	100	25.33	100
37.79	20	36.07	50	25.68	80
48.03	35	41.21	25	30.80	90
53.87	20	54.30	60	36.24	25
55.04	20	56.62	20	47.99	30
		65.45	20	51.18	20
		68.98	20	55.21	30

In anatase each Ti atom is surrounded by six oxygen atoms and each oxygen atom is surrounded by three Ti atoms thus the structure is 6:3 coordination (Fig. 7c). The location of the Ti and O atoms and the unit cell of anatase phase are presented in Fig. 7a. The bonds between Ti and O atoms are shown in Fig. 7b, and the structure of anatase with TiO<sub>6</sub> octahedra is shown in Fig. 8.

The symmetry of anatase structure decreases when  $\text{Li}^+$  enters and  $\text{Li}_x\text{TiO}_2$  ( $x=0.5$ ) forms, as the result of change in symmetry of the crystal, the volume of the unit cell increases by 4% and rapid capacity fade is followed [46]. Theoretical capacity of  $\text{TiO}_2$  is 335 mAh/g, however reaching this value is not possible unless the particles are extremely small. In that case,  $\text{Li}^+$  cannot be stored at the theoretical level and structure like  $\text{Li}_x\text{TiO}_2$  forms where  $x$  is less than 1 [47]. It was reported that nano-sized anatase at 0.1C has a first discharge capacity of 215 mAh/g, where  $\text{Li}_{0.68}\text{TiO}_2$  was formed during  $\text{Li}^+$  intercalation [48]. Some other researchers found a higher capacity of 286 mAh/g at 1.5C as a result of carbon coating of anatase [49].

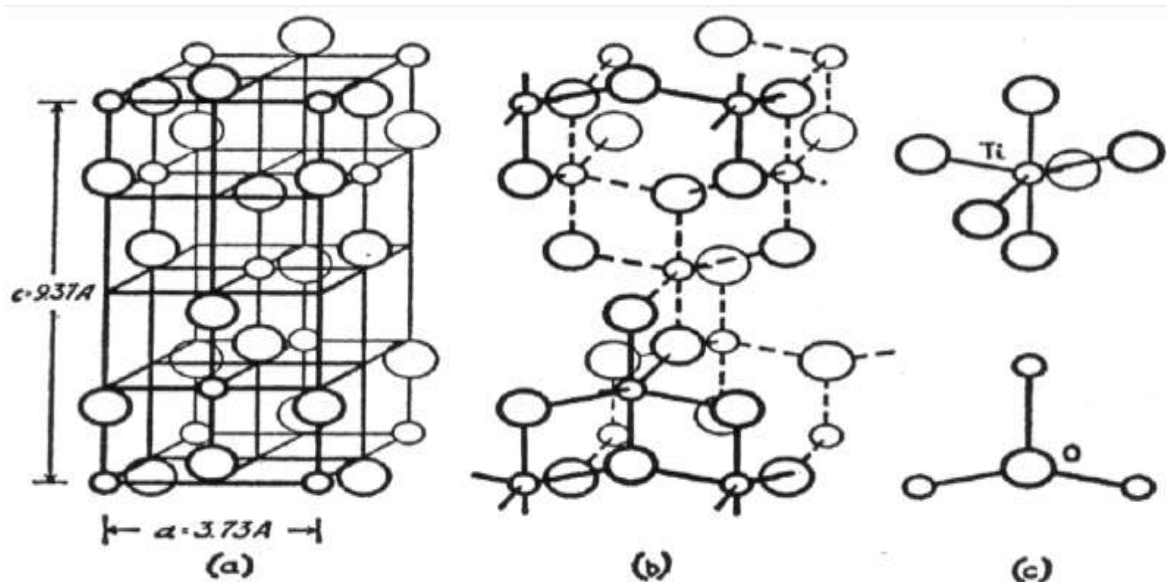


Figure 7. (a) location of Ti and O atoms in unit cell of anatase, (b) bonds between Ti and O atoms, (c) location of each Ti and O atoms [50]

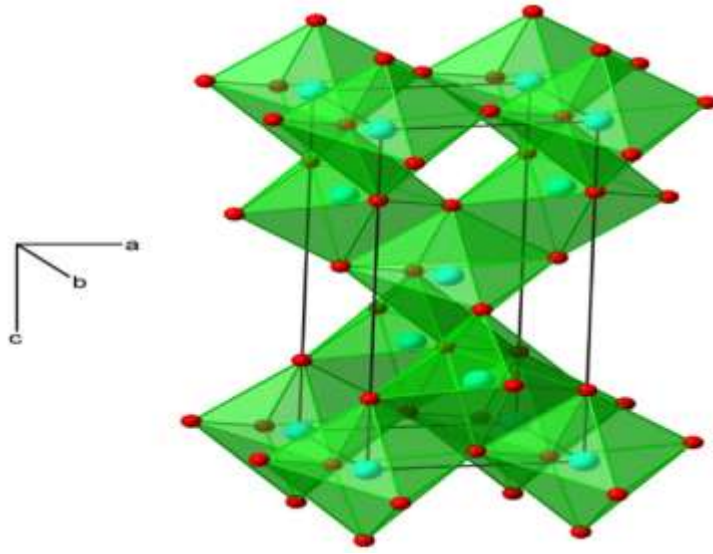


Figure 8. Anatase phase structure of  $\text{TiO}_2$  [51]

Rutile which is the most stable phase of  $\text{TiO}_2$ , has the 6:3 coordination like anatase. Its structure is shown in Fig. 9.  $\text{Li}^+$  diffusion in rutile is an anisotropic process which leads to  $\text{Li}^+$  insertion only from its c axis direction [52]. It was reported that  $\text{Li}^+$  diffusion coefficient in c axis direction is much more than ab-plane [52, 53]. Experimental data show that nano-sized rutile  $\text{TiO}_2$  has a capacity of 160 mAh/g at the rate of C/20 after 50 cycles and it decreases to 100 mAh/g at 10C [54]. It was also reported that rutile nanoparticles (15 nm) has 200 mAh/g capacity after 20 cycles at 0.3C. When the particle size was increased to 300 nm, capacity dropped to 50 mAh/g indicating that nano-sizes materials has much higher capacities [55].

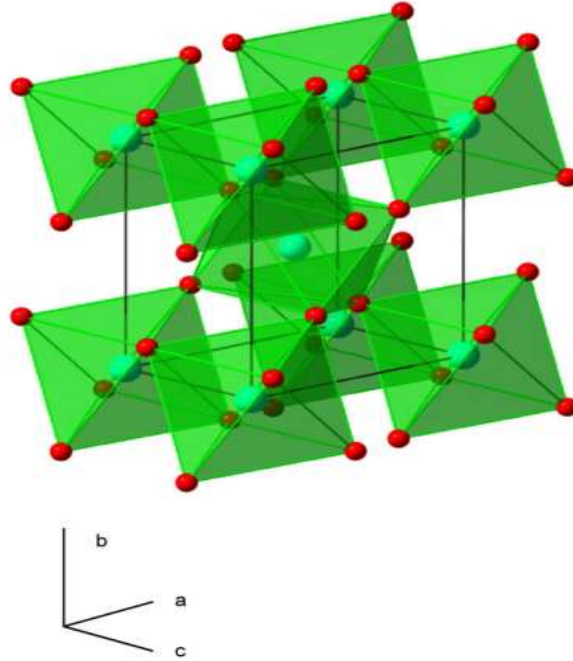


Figure 9. Rutile phase structure of  $\text{TiO}_2$  [51]

Brookite structure is orthorhombic with more complexity than anatase and rutile. Fig. 10 shows the crystal structure of brookite. Each Ti atom is enclosed by an octahedral group of oxygen atoms. Recently brookite phase has been subjected to battery testing and the results show that the performance is highly depending on the size of particles. Reported specific capacity for 10 nm brookite particles is 170 mAh/g, on the other hand, the capacity decrease to 35 mAh/g for 33 nm brookite particle sizes [56].

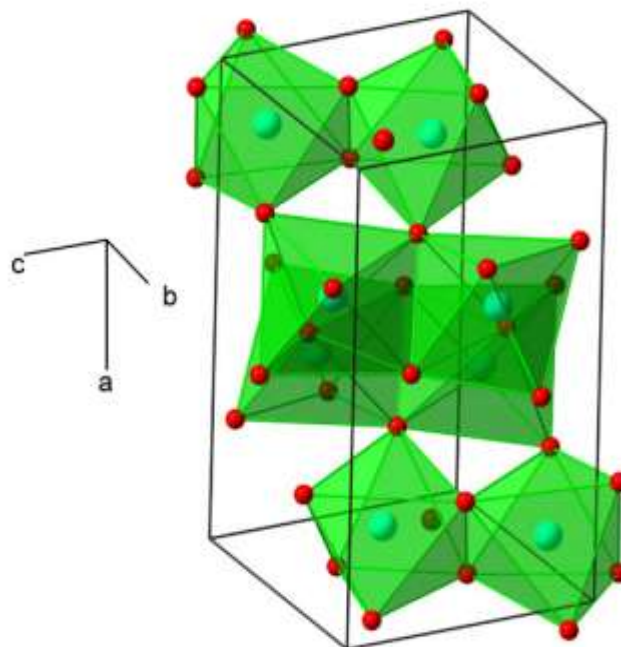


Figure 10. Brookite phase structure of  $\text{TiO}_2$  [51]

Monoclinic  $\text{TiO}_2$  (B) has the lowest density among all  $\text{TiO}_2$  polymorphs. It is mainly synthesized by acid washing of  $\text{K}_2\text{Ti}_4\text{O}_7$  to replace  $\text{K}^+$  with  $\text{H}^+$  to form hydrogen titanate, then it is transformed to  $\text{TiO}_2$  (B) after calcination at  $500^\circ\text{C}$  [57]. Structural form of  $\text{TiO}_2$  (B) is shown in Fig 11. The octahedra in  $\text{TiO}_2$  (B) align themselves to form a perovskite structure. This creates pathways for easier  $\text{Li}^+$  insertion and make this unique structure the best host for  $\text{Li}^+$  among  $\text{TiO}_2$  polymorphs [58]. Some researchers synthesized nanowires of  $\text{TiO}_2$  (B) by hydrothermal treatment of anatase  $\text{TiO}_2$  in alkali solution. They subjected the material to electrochemical testing and obtained a capacity of 305 mAh/g [58, 59]. This capacity for  $\text{TiO}_2$  (B) is much higher than the other polymorphs, but still it is far from theoretical capacity (335 mAh/g) indicating that  $x$  in  $\text{Li}_x\text{TiO}_2$  is less than 1.

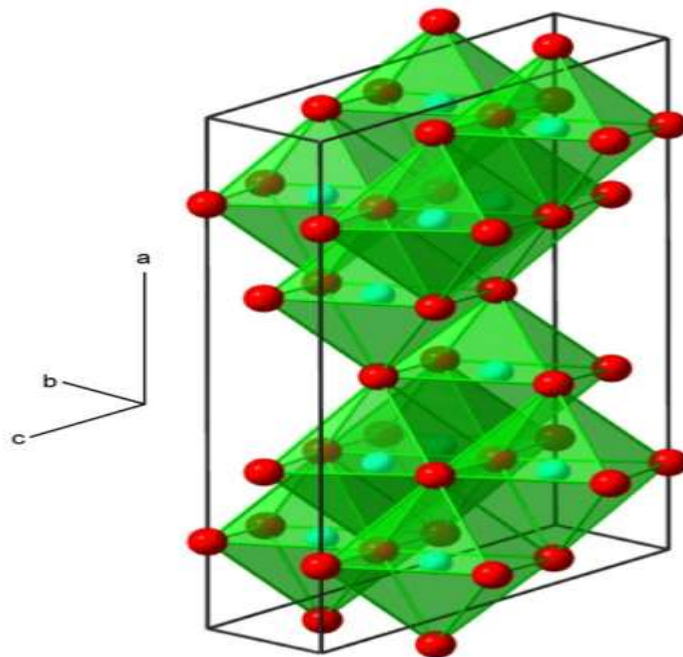


Figure 11.  $\text{TiO}_2$  (B) phase structure of  $\text{TiO}_2$  [51]

Various forms of  $\text{TiO}_2$  nanocrystals have been prepared via different experimental procedures [60, 61]. Platelets, nanorods, diamond shaped and bullet nanocrystals and nanotubes forms of  $\text{TiO}_2$  nanocrystals have been synthesized in hydrolysis reaction of titanium alkoxides [62].

It was shown that electrochemical performance, lithium insertion-deinsertion and reversible capacity of titanium dioxide anode are highly dependent on their size, structure and morphology [55]. Therefore modifying  $\text{TiO}_2$  to obtain large surface areas and high porosities can consequently result in better capacity, longer cycle life and higher rate capability. Lots of studies have been carried out to modify  $\text{TiO}_2$  into titanate nanotubes which are examined as an anode material [63, 64]

Titanate nanotubes have attracted attention due to their promising properties like high surface area and layered crystal structure which are the important factors that influence energy storage kinetics [65]. They are generally synthesized via hydrothermal treatment of  $\text{TiO}_2$  powder in an alkali solution followed by washing with acidic solutions. There are still

some debates about formation step of the nanotubes. While some studies claim that the nanotubes form during the hydrothermal treatment step, the other studies tell that they form after acid washing. In the latter claim, first layered sodium titanates ( $\text{Na}_2\text{Ti}_3\text{O}_7$ ) form during hydrothermal treatment where sodium cations ( $\text{Na}^+$ ) are between edge-shared octahedral layers ( $\text{TiO}_6$ ). Then due to high surface energy the layers scroll up to form the nanotubes [66-69]. After acid washing,  $\text{Na}^+$  are replaced with  $\text{H}^+$  leading to a decrease in interlayer distances, increase in surface area and from hydrogen titanate ( $\text{H}_2\text{Ti}_3\text{O}_7$ ) nanotubes [70, 71] where  $\text{Li}^+$  can easily move in the structure (Fig. 12).

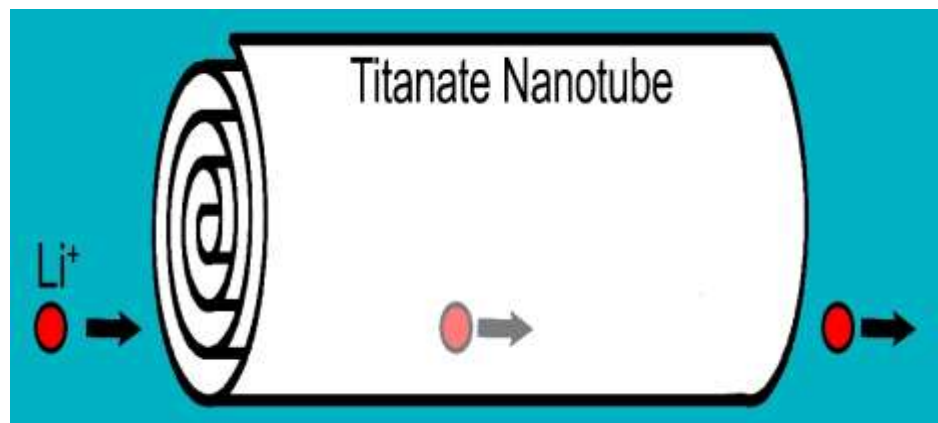
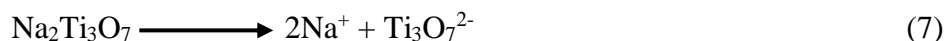


Figure 12. Scroll shape of titanate nanotube

Reaction that occurs during hydrothermal treatment is shown in equation 6. In the first step, dissolution  $\text{TiO}_2$  is followed by crystallization of layered sodium titanate ( $\text{Na}_2\text{Ti}_3\text{O}_7$ ). In the next steps, treatment with acidic solutions leads to ion exchange forming  $\text{H}_2\text{Ti}_3\text{O}_7$  (equations 7, 8, 9). Here  $\text{H}_2\text{Ti}_3\text{O}_7$  has a zig-zag  $(\text{TiO}_6)_n$  layered structure like  $\text{Na}_2\text{Ti}_3\text{O}_7$ , however the interlayer distance is shorter (Fig. 13).



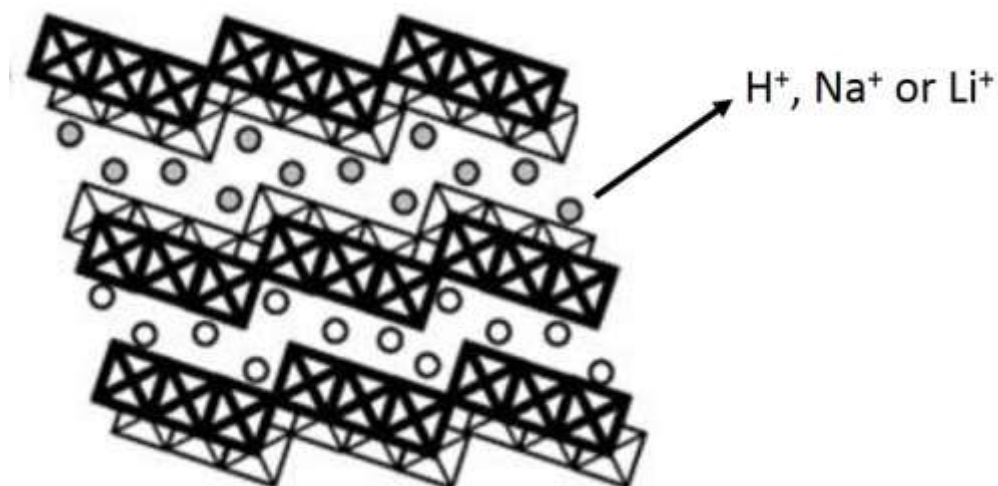


Figure 13.  $\text{Li}^+$  intercalated zig-zag layers structure of titanate with  $\text{Li}^+$ ,  $\text{H}^+$  and  $\text{Na}^+$  between its layers [72]

Titanate nanotubes are widely tested as an anode active material in LIBs due to their layered structure that facilitates  $\text{Li}^+$  insertion-deinsertion. Titanates are considered as a pseudocapacitive metal oxide in which redox reactions take place at or near the surface which leads to fast charge-discharge process and provide high power densities [73].

There are some studies that have been conducted on hydrogen titanate nanotubes synthesized via hydrothermal treatment and their electrochemical performances. Table 3 summarizes the hydrothermal treatment conditions and the electrochemical properties of these hydrogen titanate nanotubes. In all of these studies anatase  $\text{TiO}_2$  nanoparticles were hydrothermally treated with 10 M NaOH in a Teflon-lined autoclave.

Table 3. Electrochemical properties of hydrothermally treated TiO<sub>2</sub>

Titanate morphology	Temp. (°C)	Duration (h)	1 <sup>st</sup> discharge Capacity (mAh/g)	Current density (A/g)	Reference
Nanotubes	150	48	330	0.05	[74]
Nanowires	150-180	> 72	191	0.3	[75]
Nanotubes	120	> 48	210	0.24	[76]
Nanotubes	110	22	182	0.08	[77]
Nanorods	110	48	174	0.05	[78]
Nanowires	200	72	220	0.05	[79]
Nanowires	170	> 72	100	40	[80]
Nanotubes	110	24	168	0.21	[81]

It can be seen from Table 3 that titanates with different morphologies can be obtained hydrothermally in the temperature range of 110-180°C between 1-3 days. The morphology of titanates improved the capacity when the performance is compared with TiO<sub>2</sub> nanoparticles. Nanotubular structure allows Li<sup>+</sup> to flow easily in the lattice and with its pseudocapacitive properties the material shows higher power densities.

As a precursor of titanates, surface area, pore size, particle size and crystallinity of TiO<sub>2</sub> highly affect the properties of titanates after hydrothermal treatment. The final morphology and textural properties are very crucial parameters, since they directly affect the electrochemical performance. For that reason, it is crucial to control the particle size, shape

and porosity of  $\text{TiO}_2$  for titanate synthesis. The easiest way to achieve this is to synthesize  $\text{TiO}_2$  with sol-gel method.

#### 1.4.2. Sol-gel method

There are different methods to obtain metal oxides; such as microemulsion, hydrothermal and sol-gel synthesis. Microemulsion synthesis is a method for the synthesis of metal oxides with different particle sizes in water-oil emulsions. Some surfactants are used to control particle sizes. Applications of microemulsion materials are more in biological fields like drug delivery [82]. Hydrothermal synthesis method is based on chemical reactions of substances in an aqueous solution which is heated above room temperature in a high pressure sealed vessel to grow nanocrystals. Supercapacitors and catalysts can be considered as the important applications of hydrothermal synthesized metal oxides [83]. Nowadays, sol-gel technique is widely used for the synthesis metal oxides ( $\text{Fe}_2\text{O}_3$ ,  $\text{TiO}_2$ ,  $\text{Al}_2\text{O}_3$ , etc) with several benefits [84-86]. The process parameters are easier to control and the materials obtained have better homogeneity, higher porosity with a low cost [87]. General schematic representation of this process can be seen at Fig. 14.

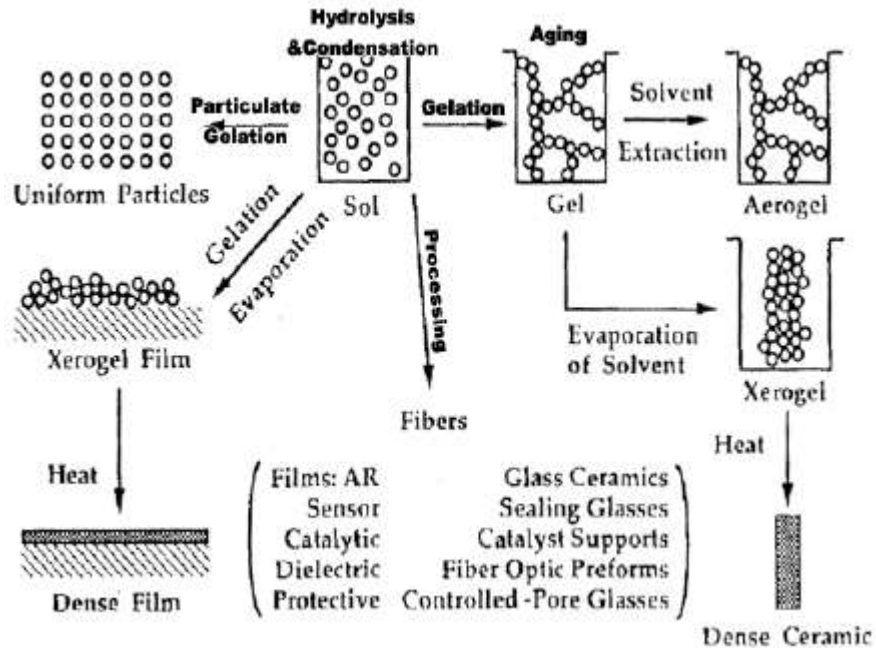


Figure 14. Schematic presentation of sol-gel process [88]

TiO<sub>2</sub> nanoparticles are widely synthesized via sol-gel technique. Titanium alkoxides as well as non-alkoxides are used as titanium precursors in the synthesis of TiO<sub>2</sub>. The most widely used alkoxide precursors are TiCl<sub>4</sub> [89], Ti(i-OP)<sub>4</sub> [90] and Ti(OBu)<sub>4</sub> [91]. In this process, TiO<sub>2</sub> is generally formed via 2 important reactions, hydrolysis and polycondensation reactions. Titanium precursor Ti(OR)<sub>n</sub> reacts with water to produce oxopolymers in aqueous phase, then these products are finally transformed into an oxide state. When titanium hydroxide forms, the first step of the reaction comes to an end (equation 10).



After the formation titanium hydroxide, the polymerization reactions take place.

Condensation dehydration



Dealcoholation



And the overall reaction is as following



Particles agglomerate to form metal oxide crystal in the condensation reactions [92]. After that, gelation of the solute occurs where a three-dimensional state of gel forms. This step is important in terms of controlling the structure of the final product. Evaporation of water and alcohol starts after gelation; as a consequence the gel shrinks and creates pores.

The morphology of the final  $\text{TiO}_2$  nanoparticles is highly affected by different factors such as titanium precursors [93], drying step temperature [94] and reaction pH value [95]. Calcination is also one of the main factors that affect final  $\text{TiO}_2$  nanoparticles. In calcination, the amorphous powder is heated under oxygen environment to crystallize the inorganic compounds. High calcination temperature leads to loss some hydroxyl groups and decrease in surface area. It was reported that low calcination temperature as low as  $300\text{ }^\circ\text{C}$  can be used to crystallize dried  $\text{TiO}_2$  [96].

Titanate nanotubes as a titania based materials, have some unique structural properties like high surface area, layered crystal structure and high porosity. These properties can make titanate nanotubes a promising anode material. Sol-gel method just yields  $\text{TiO}_2$  polymorphs, while titanate nanotubes can be easily synthesized hydrothermally [97].

#### 1.4.3. Hydrothermal Treatment

Hydrothermal treatment can be defined as heterogeneous reactions in aqueous media over  $100\text{ }^\circ\text{C}$  and above 1 atm. The advantages of hydrothermal treatment is proving high surface

area with porous structures which are suitable to be used as anode in LIBs [83]. This technique is generally used for metal oxides and hydroxide nanoarrays. Single crystal metal oxides ( $\text{Co}_3\text{O}_4$ ,  $\text{ZnO}$ ,  $\text{TiO}_2$ ,  $\text{V}_2\text{O}_5$ ,  $\text{Fe}_2\text{O}_3$ ,  $\text{Fe}_3\text{O}_4$ , etc) are synthesized with this method to enhance their structural properties [83]

To obtain titanate nanotubes ( $\text{H}_2\text{Ti}_3\text{O}_7$ ), anatase  $\text{TiO}_2$  nanoparticles should be reacted hydrothermally with  $\text{NaOH}$  solution in a Teflon-lined autoclave.  $\text{NaOH}$  concentration should be more than 5 M while temperature should be at least  $100^\circ\text{C}$  then the as-prepared product should be washed with acidic solutions and deionized water to reach the neutral pH conditions [71]. Hydrothermal treatment is commonly used to produce titanate nanotubes due to its noticeable advantages like low energy requirement, high reactivity and also its easiness of controlling the aqueous solution [98]. Temperature, duration and pH value of the post-treatment step highly affect the final product's characteristics. Figure. 15 represent a schematic mechanism of formation titanate nanotubes.

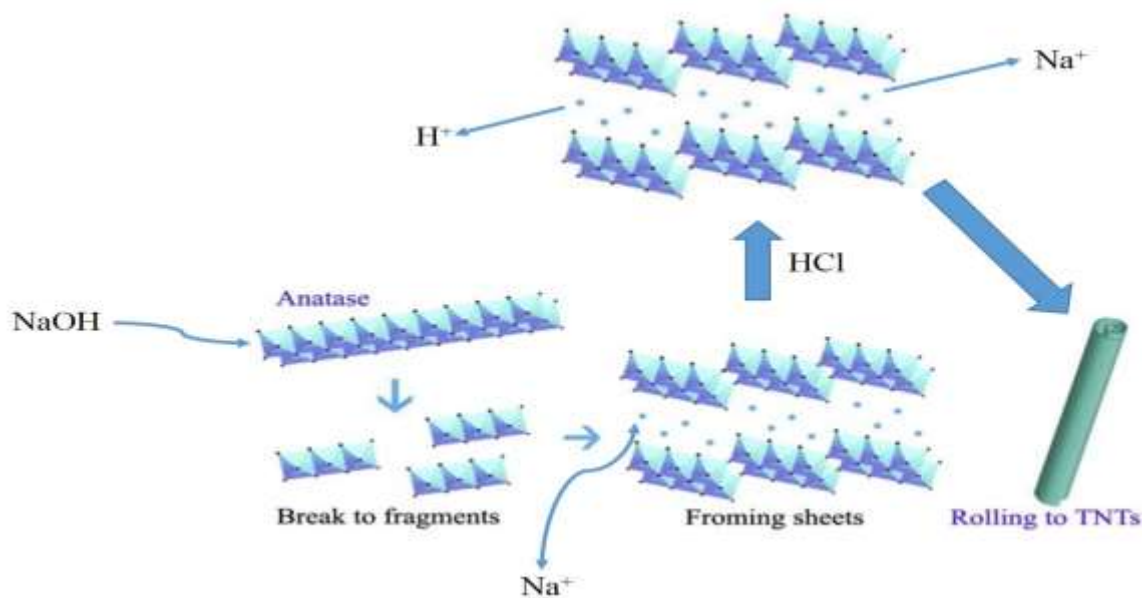


Figure 15. Schematic formation mechanism of titanate nanotubes [64]

The hydrothermal treatment temperature has a significant impact on the crystal growth of  $\text{H}_2\text{Ti}_3\text{O}_7$ . The higher the temperature is, the more degree of crystallinity can be obtained

[99]. It should be done in the range of 100-180°C to form titanate nanotubes. It was reported that at the temperature range of 100-150°C, the highest yield of nanotubes can be obtained [100]. Some researchers found that the highest pore volume and surface area of titanate can be obtained when the hydrothermal treatment is conducted at 130°C [101].

During acid washing step, Na<sup>+</sup> which are located between titanate layers are replaced with H<sup>+</sup>, as a result while the surface area increases and the interlayer distances decrease. Some researchers have synthesized titanate nanotubes via hydrothermal treatment at 150°C, then they washed the product in 0.1 M HCl. They observed that nanotubes became shorter and also the lowest surface area and pore volume belong to samples that have the least sodium amount in their structure [98]. Table 4 summarizes some studies that were successful to obtain titanate nanotubes by using different precursors which were treated with 10 M NaOH in the temperature range of 130-180°C and duration of 1-3 days. In cases where post-treatment were needed, first samples were washed with 0.1 M HCl solution then deionized with water to reach pH 7.

Table 4. H<sub>2</sub>Ti<sub>3</sub>O<sub>7</sub> nanotubes prepared by different TiO<sub>2</sub> precursors, experimental and post-treatment conditions

precursor	Temp.(°C)/ duration (h)	post-treatment	nanotube diameter(nm)	reference
anatase	130/72	water	9	[102]
anatase	130/72	HCl + water	9	[103]
anatase	130/72	HCl + water	10	[63]
anatase	180/48	water	10	[104]
anatase	180/24	HCl + water	10	[105]

anatase/rutil	150/20	water	12	[106]
rutile	150/72	HCl + water	8	[99]

---

In this study, by changing the pH values of the post-treatment step, the nanotube diameter has been changed; and as consequence the interlayer distances and surface area have been changed as well. These parameters significantly affect electrochemical performance of titanate nanotubes. High mobility of  $\text{Li}^+$  in the structure of titanates can be achieved by increasing the interlayer distances. This goal can be obtained by hydrothermally treating titanates with surfactants. This surfactant treatment process has never been tried for titanate nanotubes before.

#### 1.4.4. Surfactant treatment

Surfactants are generally organic compounds that have water soluble and insoluble parts. They contain hydrophilic groups (the head) and hydrophobic groups (the tail). In some studies Cationic and anionic surfactant were used with layered titanates to obtain hybrid organic-inorganic films [107]. In this study, we used surfactant to modify the structure of titanate nanotubes to obtain better anode materials. Modification of titanate nanotubes with surfactants can be useful to store more  $\text{Li}^+$  between titanate layers. By increasing the interlayer distances of titanate nanotubes, this goal can be achieved. Treating layered titanates with surfactants under hydrothermal conditions replaces  $\text{H}^+$  or  $\text{Na}^+$  between the layers with long surfactant chains, thus with this technique expanded nanotubes can be obtained.

## 1.5. Objectives

*The main objectives of this work are listed below*

- Synthesizing high surface area anatase TiO<sub>2</sub> nanoparticles via sol-gel method.
- Titanate nanotubes with high specific surface area and layered structure can have remarkable electrochemical performance, thus the next aim is modify the interlayer distance of titanate nanotubes with acid washing to enhance Li<sup>+</sup> mobility for high power density and good rate capabilities.
- Re-modify the titanate nanotube structure using surfactants to obtain expanded titanate nanotubes.

*Remarkable novelties of this work are:*

- Modification of titanate nanotubes' interlayer distances by post-treatment to prepare titanate nanotubes washed in a wide range of pH values.
- Investigation of electrochemical performance of resultant anode materials.
- Modification of titanate nanotube structure by surfactant treatment.

## 2. Materials and Methods

TiO<sub>2</sub> nanoparticles (anatase) were firstly synthesized via sol-gel method then this sol-gel synthesized TiO<sub>2</sub> and commercial TiO<sub>2</sub> (anatase) were used as two different TiO<sub>2</sub> sources to be treated with a basic solution hydrothermally to obtain titanates. Moreover, these titanates were modified by hydrothermally treating with surfactant. All of the samples were subjected to morphology and electrochemical testing characterizations.

### 2.1. Sol-gel synthesis

TiO<sub>2</sub> nanoparticles were synthesized by utilizing titanium isopropoxide (TTIP) (Sigma–Aldrich CAS no: 546-68-9) as a precursor. 8.4 mL of TTIP was diluted in 20 mL of 2-propanol (Aldrich CAS no: 67-63-0) then a solution of 0.25 mL of HCl (Aldrich CAS no: 7647-01-0), 0.5 of distilled water and 130 mL of 2-propanol was slowly added to the first solution to initiate the reaction. After the complete addition of the second solution, the mixture was left for aging under constant stirring for 1 hour at room temperature. After that, the TiO<sub>2</sub> sol was dried for 2 days at 60°C then the dried sample was subjected to Protherm calcination furnace (Fig.16) with air flow for 4 hours at 450°C in order to obtain anatase phase of TiO<sub>2</sub>. Fig. 17 represents mechanism of sol-gel synthesis.



Figure 16. Protherm calcination furnace

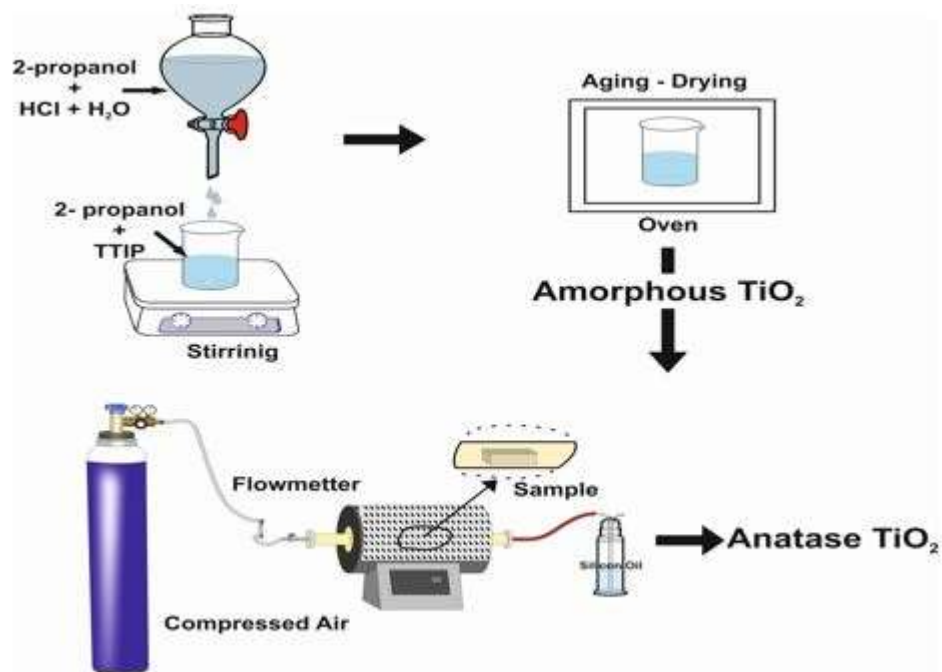


Figure 17. Schematic mechanism of sol-gel method

## 2.2. Hydrothermal treatment

Anatase TiO<sub>2</sub> nanoparticles which have been synthesized with sol-gel technique and commercial anatase (Aldrich CAS no: 1317-70-0) were used here as the starting materials. 1.5 g of either sol-gel or commercial anatase were dispersed in an aqueous solution of 120 mL 10 M NaOH (Aldrich CAS no: 1310-73-2) and stirred for 30 min. After that, the solution was put in a Teflon-lined autoclave (Fig. 18), heated to 130°C and hydrothermally treated for 48 hours. The final solution was then filtered and dried at 110°C for 3 hours. The dried filter cake was powdered and added to 1 L water having different pH values (the pH was adjusted using 0.1 M HCl) for 20 hours in order to replace Na<sup>+</sup> with H<sup>+</sup>. Finally the washed sample was again filtered and dried at 110°C for 3 hours to obtain hydrogen titanate (H<sub>2</sub>Ti<sub>3</sub>O<sub>7</sub>). Fig. 19 shows the hydrothermal treatment process.



Figure 18. Teflon-lined autoclave

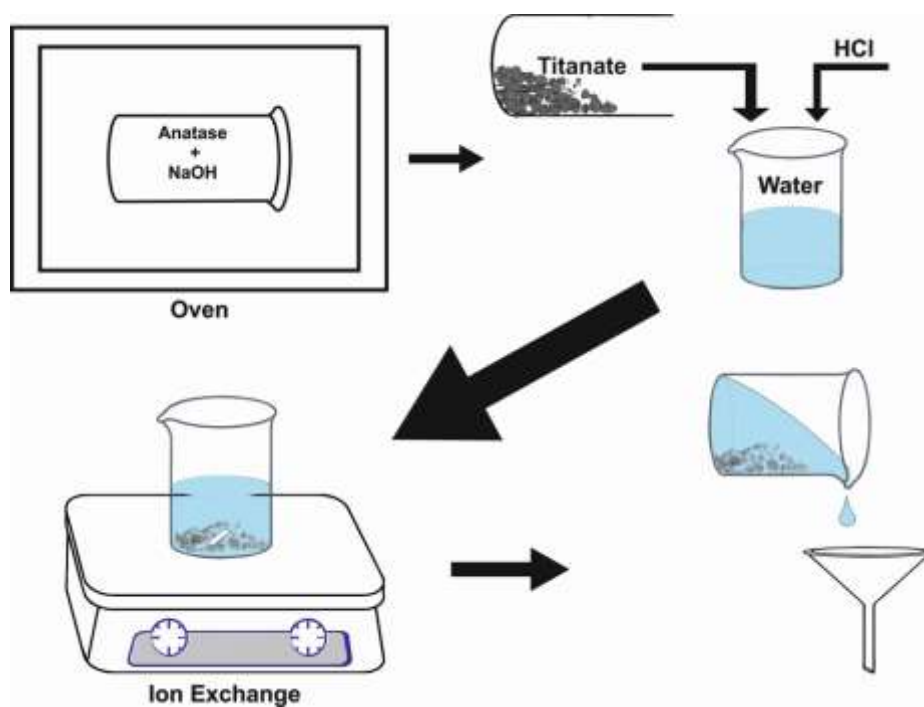


Figure 19. Schematic mechanism of hydrothermal treatment

### 2.3. Surfactant treatment

1 g of titanate which has been synthesized hydrothermally, 8 mL of dodecylamine ( $C_{12}H_{27}N$ ) as surfactant and 10 mL of ethanol were subjected to a Teflon-lined autoclave and they were hydrothermally treated at  $130^{\circ}C$  for 48 hours then the solution was mixed with water:ethanol ratio of 1, then the solution was stirred for 30 min. after that, the final product was filtered and dried at  $90^{\circ}C$  for 3 hours. In this process  $H^{+}$ , which are placed between titanate layers are replaced with surfactant cations. Fig. 20 represents the surfactant treatment mechanism.

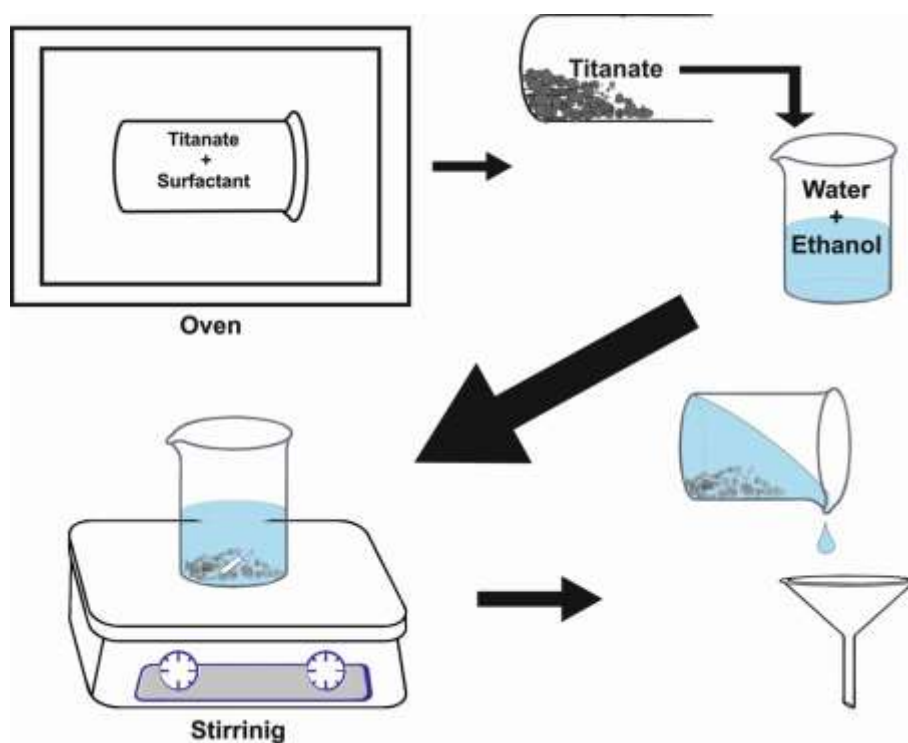


Figure 20. Schematic mechanism of surfactant treatment

### 2.4. Structural characterization

For the x-ray diffraction (XRD) analysis of the samples, a Rigaku Rint2000 diffractometer with a monochromatized  $CuK_{\alpha}$  irradiation ( $\lambda = 0.15405nm$ ) was used. The morphology of the samples were examined by scanning electron microscopy (SEM) using a Zeiss LEO Supra 35VP SEMFEG. Surface area and pore sizes of all samples were determined using a

Quantachrome NOVA 2200e surface area and pore size analyzer in boiling N<sub>2</sub> temperature (77 K). All of the samples were degased at 150°C for 24 hours.

## 2.5. Electrochemical characterization studies

A mixture of active material (75 wt.% ), carbon black (20 wt.%) and poly(vinylidene fluoride) (PVDF) (5 wt.%) is prepared then it was left for 20 hours at room temperature in order to dry, then it was mixed with n-methyl-2-pyrrolidone (NMP) to obtain a past, after that the copper foil (Fig. 21a) was coated by the mixture and coated copper foil was dried at 120°C for 24 hours, then dried coated copper foil (Fig. 21b) was put in the glove box in order to assemble a lithium ion battery (Fig. 22). The battery was made of coated copper foil as anode, lithium chip (Fig. 21c) as cathode, Li-ion Battery Separator Film (25µm thick x 85mm W x 60m L, Celgard) (Fig. 21d) and lithium hexafluorophosphate solution in ethylene carbonate and dimethyl carbonate, 1.0 M LiPF<sub>6</sub> in EC/DMC=50/50 (v/v), (battery grade-746711-100ML Sigma - Aldrich) as electrolyte. Fig. 23 shows the preparation of anode.

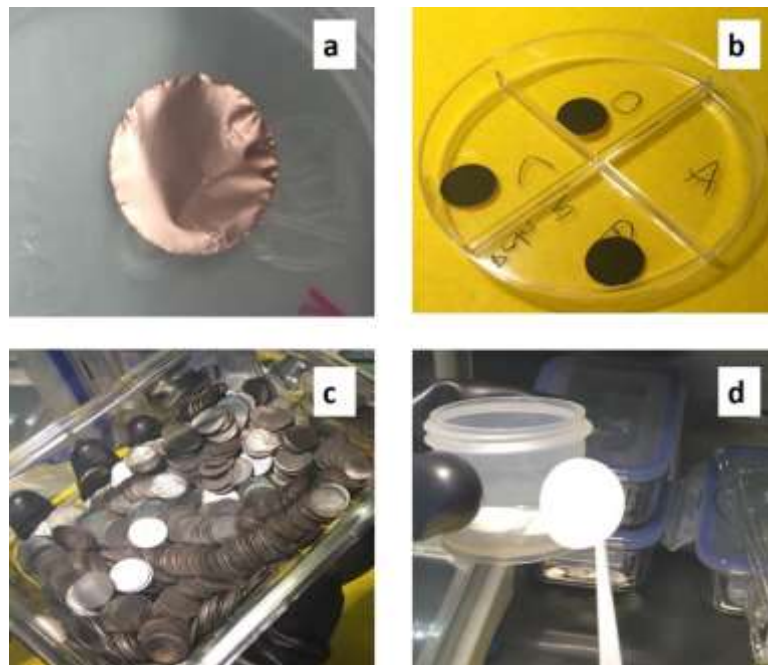


Figure 21. a) Copper foil, b) coated copper foil, c) lithium chip and d) separator



Figure 22. Assembled lithium-ion battery

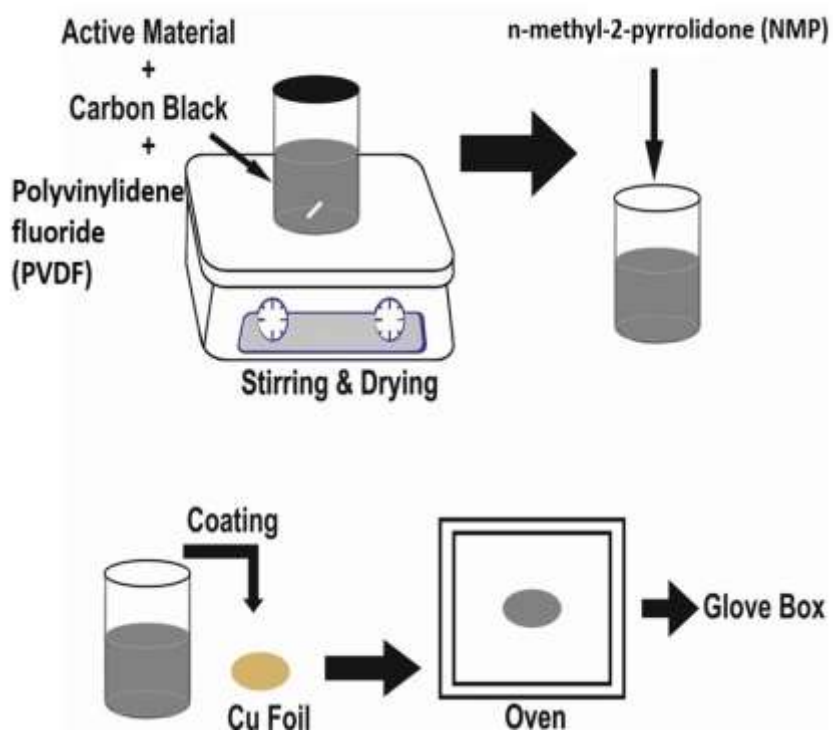


Figure 23. Preparation of anode

Assembled battery was electrochemically examined by electrochemical characterizations with constant voltage range (1-3 V)

Charge-discharge characterization was done at 0.1C, 0.5C and 1C current rates for 20 cycles. Rate capability performance was tested for 50 cycles, first ten cycles (at 0.1C), next ten cycles (at 0.5C), next ten cycles (at 1C), next ten cycles (at 5C) and last ten cycles (at 0.1C). Cyclic Voltammetry was performed with scan rate of 0.1 mV/s

### 3. Results and discussion

#### 3.1. Structural and electrochemical properties of TiO<sub>2</sub> samples

To obtain titanate nanotubes, the starting material has to be TiO<sub>2</sub>. During the nanotube synthesis, the particle size, porosity and crystal phase play an important role to achieve the product with high yields. For the aim of testing the effect of particle size, two different TiO<sub>2</sub> sources were utilized. The TiO<sub>2</sub> nanoparticles used for this purpose are sol-gel synthesized TiO<sub>2</sub> (SG) and commercial TiO<sub>2</sub> (Com).

##### 3.1.1. Thermal characterization

Since, for the titanate synthesis, the crystal phase of starting material determines the final product, deciding on the calcination temperature is important. For that purpose, the gel obtained after sol-gel synthesis was dried 60 °C and TGA/DTA analysis of that amorphous powder was made. Fig. 24 shows the TGA/DTA curves of the powdered gel TiO<sub>2</sub>. As it can be seen there are three main weight loss regions at temperatures of 130, 130-212 and 212-365 °C corresponding to vaporization of most solvents, removal and thermal decomposition of organic solvents and loss of carbon groups in the sample, respectively. DTA curve shows four endothermic peaks. The first two at the temperatures of 130 and 217 °C were associated with removal of adsorbed water on the surface of particles and evaporation of organic compounds, respectively. Exothermic peak at 370 °C was attributed to energy release during the combustion of organic matter. The third endothermic peak at 450 °C was assigned to the phase transformation of amorphous TiO<sub>2</sub> to anatase phase of TiO<sub>2</sub>. Finally the last endothermic peak at 610 °C was attributed to the phase transformation from anatase to rutile [108]. To obtain trititanate (H<sub>2</sub>Ti<sub>3</sub>O<sub>7</sub>) nanotubes, pure anatase is the preferred starting material. For that reason, calcination temperature should not exceed 610 °C. In addition to that, to reduce sintering problems it was decided to perform calcination at 450 °C.

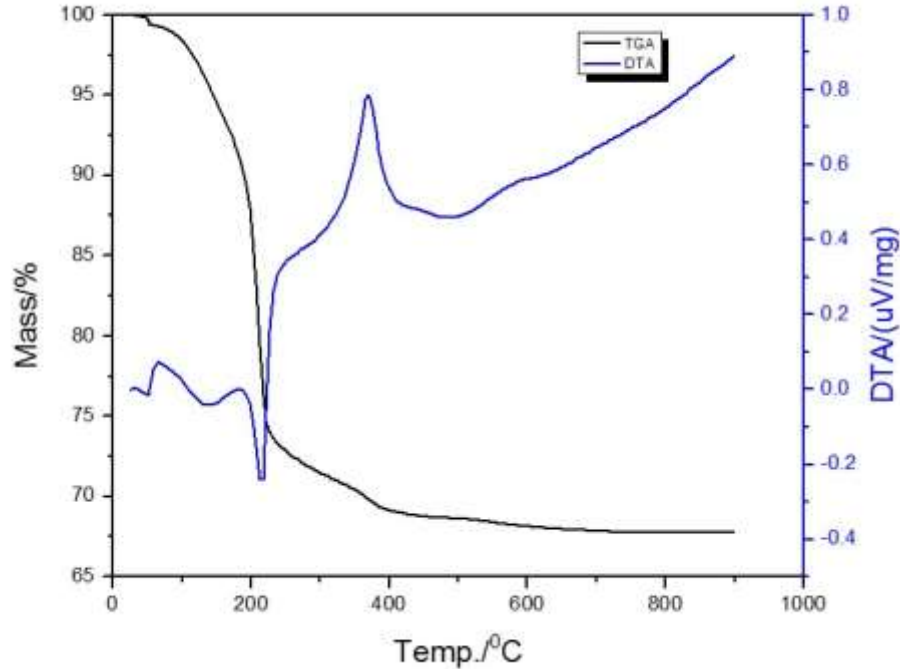


Figure 24. TGA/DTA curves of SG

### 3.1.2. XRD characterization

XRD patterns of as-prepared nano-TiO<sub>2</sub> (SG) and commercial anatase (Com) are shown in Fig.25. All peaks are in good agreement with the standard anatase spectrum (JCPDS no.: 84-1286) and no other phase of TiO<sub>2</sub> was observed. Also the main peak of anatase (101) at  $2\theta = 25.4^\circ$  was used for finding the crystallite sizes of the samples utilizing the Scherer's equation [109, 110]. The crystallite sizes of SG and Com were calculated as 17 nm and 65 nm, respectively. The patterns show that SG and Com is suitable for titanate nanotube synthesis. If the particles of a material is big, the crystallite size does not directly give the particle size. However it gives a general idea and from calculated crystallite sizes it can be suggested that SG and Com will yield different structures since the particle size of TiO<sub>2</sub> also affects the morphology of titanate nanotubes.

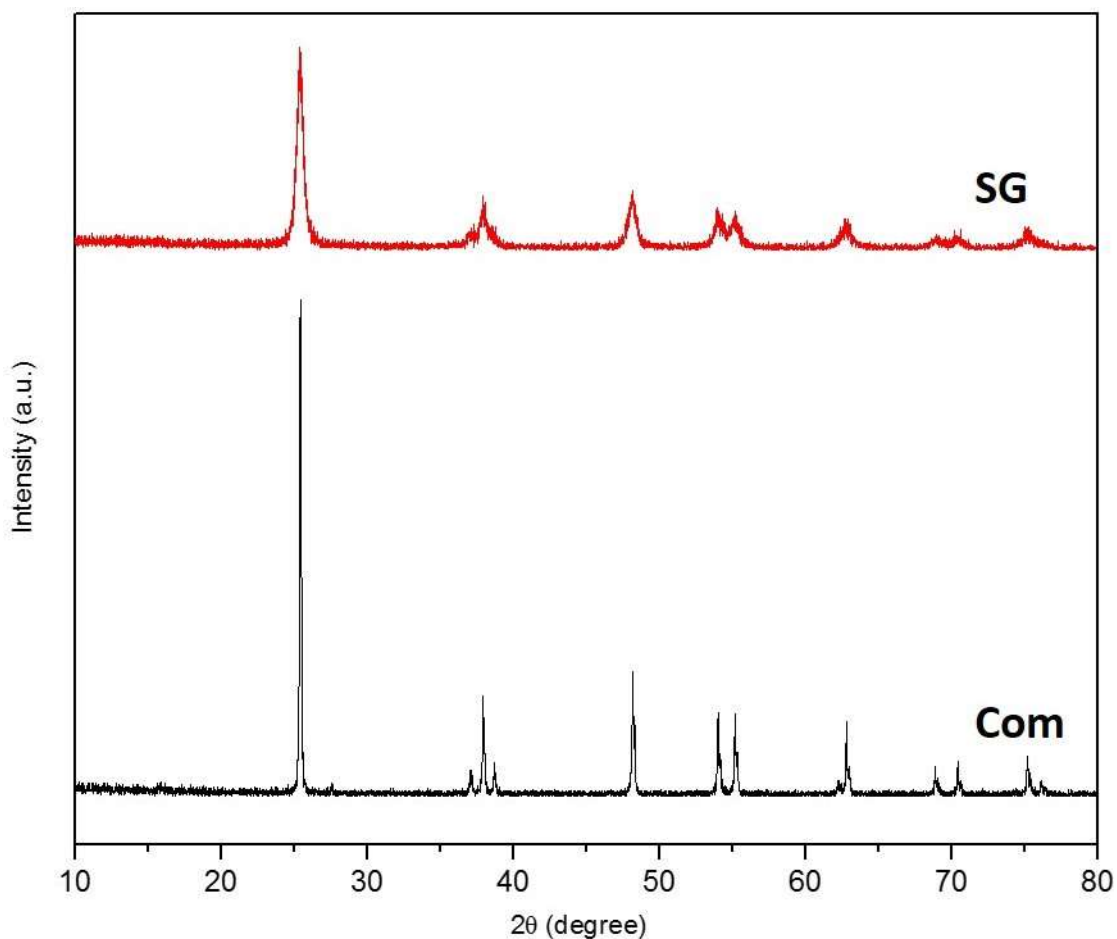


Figure 25. XRD diffraction patterns of Com and SG

### 3.1.3. SEM characterization

As mentioned at the previous section, the morphology of  $\text{TiO}_2$  is important since it determines the final structure of titanate nanotubes. For that reason, morphologies of SG and Com were studied by SEM (Fig. 26). Agglomerated SG nanoparticles have average particle size of 20 nm which is consistent with literature that reported 15-20nm [109], 20nm[111] and 25nm [112] particle sizes for sol-gel anatase calcined at 450 °C. It should be also noted that the crystallite size calculated for SG is close to its particle size. In contrast to SG, the average particle size of Com is 140 nm. As can be seen from the SEM images, Com has macroporous (pores bigger than 50 nm) structure. On the other hand, SG, has micro and mesopores (pores smaller than 2 nm and pores between 2 and 50 nm) (which will be discussed in the following section). Although having a small particle size is better

for achieving high reaction rates, the highly agglomerated SG can delay the formation of titanates under hydrothermal conditions.

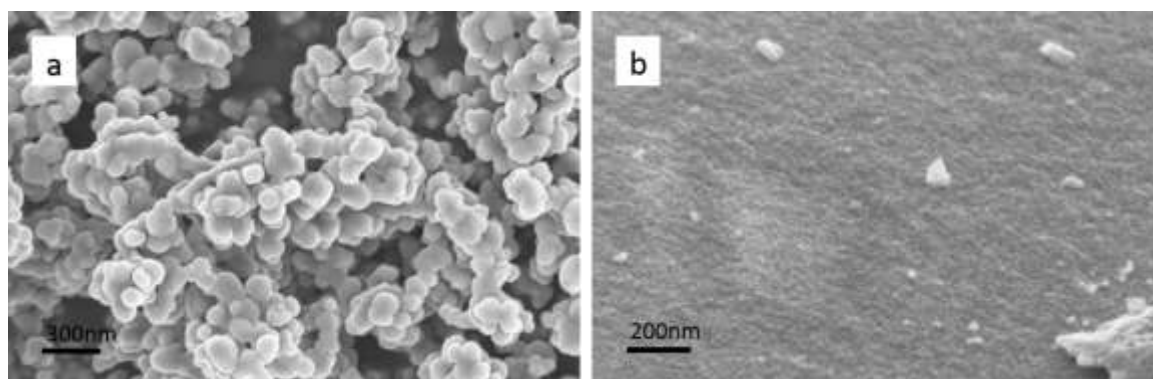


Figure 26. SEM images of a) Com, and b) SG

#### 3.1.4. Surface area and pore size analyses

Not only for the electrochemical performance but also for the hydrothermal reactions, high specific surface area and the porosity is desired. To determine the surface area and the porosities BET and BJH analyses were made. Specific surface areas of SG and Com were measured as  $63 \text{ m}^2/\text{g}$  and  $13 \text{ m}^2/\text{g}$ , respectively. In addition, the pore volume of SG is  $0.104 \text{ cm}^3$  and  $0.059 \text{ cm}^3$  for Com. The BJH pore size distribution curves of SG and Com clearly shows that while SG is mainly mesoporous, Com is mainly macroporous (Fig.27). It was reported that increase in calcination temperature, due to sintering, leads to larger particles, pore volumes and lower surface areas [113]. Y. Li and his co-workers calcined sol-gel synthesized amorphous  $\text{TiO}_2$  at  $300 \text{ }^\circ\text{C}$  and  $700 \text{ }^\circ\text{C}$ . Their surface area results were  $171 \text{ m}^2/\text{g}$  for  $300 \text{ }^\circ\text{C}$  and  $2 \text{ m}^2/\text{g}$  for  $700 \text{ }^\circ\text{C}$ . In another study, again sol-gel  $\text{TiO}_2$  they obtained surfaces areas in the range of  $53 - 45 \text{ m}^2/\text{g}$  after calcination performed at the temperatures between  $400 - 500 \text{ }^\circ\text{C}$  [114]. In addition to being consistent with our SG sample, it was seen that temperature has a significant effect on surface area.

During the hydrothermal synthesis of titanate nanotubes, after reaching supersaturation dissolution/recrystallization reactions occur. At such conditions, the mesoporous structure of SG may decrease those reactions and delay the formation of the nanotubes. However, for

electrochemical studies, this problem does not exist and SG should have better capacity than Com with its larger specific surface area.

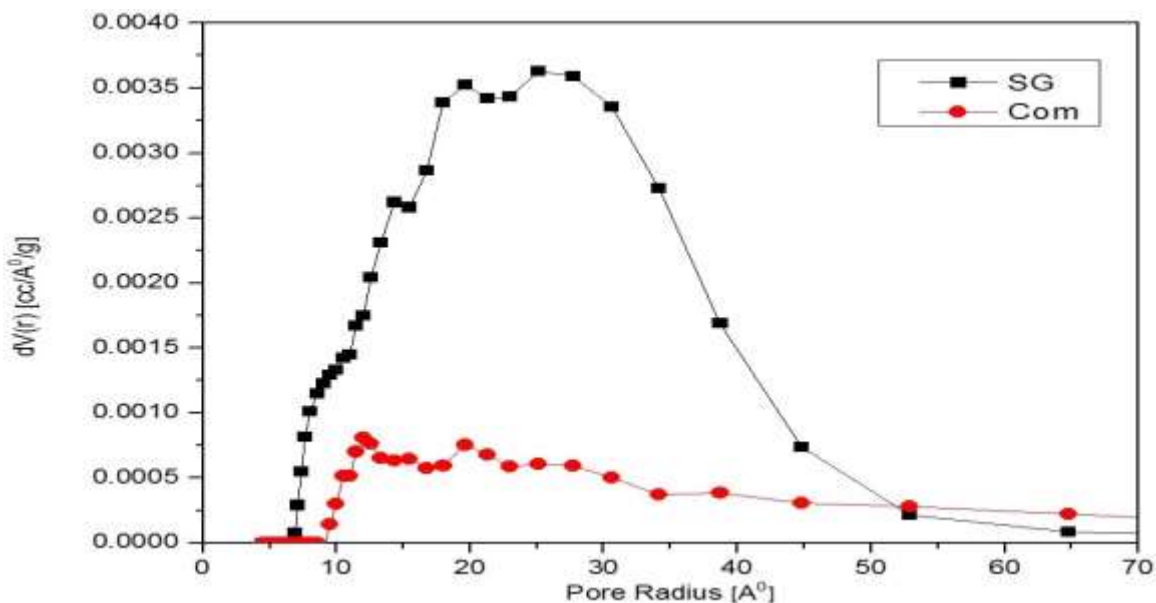


Figure 27. Pore size distributions of Com and SG using BJH method

### 3.1.5. Electrochemical characterization

To make a comparison with titanate nanotubes, electrodes were also made out of SG and Com. The cyclic voltammogram curves of the first cycle for both Com and SG are shown in Fig. 28. For Com, the  $\text{TiO}_2$  oxidation of  $\text{Ti}^{3+}$  to  $\text{Ti}^{4+}$  occurs at 2.14 V and corresponding reduction takes place at 1.68 V. In the case of SG the oxidation and reduction take place at 2.3 V and 1.51 V, respectively which are consistent to faradic deinsertion and insertion of  $\text{Li}^+$  to anatase [115]. When compared with Com, SG had wider oxidation-reduction peaks indicating slower insertion kinetics for SG [116]. SG is a mesoporous material with high agglomeration, which delays  $\text{Li}^+$  insertion. On the other hand, lower peak potential separation of Com (0.46 V) than the predicted Faraday's law (0.59 V) means there were some side-reaction during lithium insertion into Com lattice [117]. These values are also consistent with constant voltage plateaus obtained at charge-discharge curves.

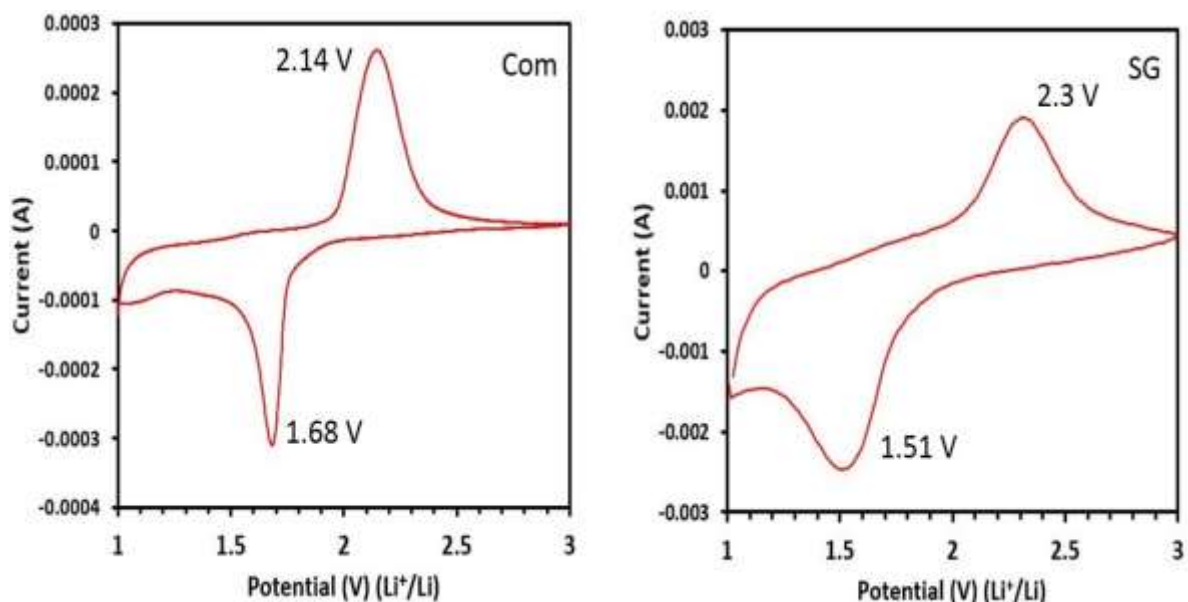


Figure 28. Cyclic voltammetry of Com and SG

Fig. 29 (a, b) shows the first three charge-discharge profiles of Com and SG electrodes, respectively. In the first discharge of both materials, three regions can be distinguished: the first region is at higher voltages before a constant voltage plateau at 1.75 V. In this region, potential drops as the result of formation of  $\text{Li}_x\text{TiO}_2$  [118] the extent of this region is related to the surface area of the material. The second region is the constant voltage plateau at 1.75 V, this plateau is due to the formation of two phases of  $\text{Li}_{0.6}\text{TiO}_2$  (lithium rich) and  $\text{Li}_{0.01}\text{TiO}_2$  (lithium poor) [119], in other words, during  $\text{Li}^+$  insertion, anatase changes to two phases which one of them is lithium poor with tetragonal symmetry and another one is lithium rich with orthorhombic symmetry. The third region is voltages less than 1.75 V, in this region  $\text{Li}^+$  is stored at the surface of the material thus extension of this region is dependent on the surface area of the materials. As can be seen from Fig. 29 (c) The discharge capacities of Com electrode at current rate of 0.1C in the first and twentieth cycles are 256 mAh/g and 54 mAh/g, respectively, while these values for SG (Fig. 29d) are 357mAh/g and 104 mAh/g, respectively. The higher first discharge capacity as well as reversible capacity for SG are due to smaller particle size and larger surface area of SG when compared with Com [120]. Although the theoretical capacity of anatase  $\text{TiO}_2$  is 335 mAh/g only half of this capacity can be achieved (165 mAh/g) for large particles because presence of  $\text{Li}^+$  in

$\text{Li}_x\text{TiO}_2$  (where  $x$  is higher than 0.5) leads to high Li-Li interaction in the lattice thus  $\text{Li}^+$  just store only in half of the octahedral interstices [47, 121]. However since Com has much bigger particles, even half of these octahedral spaces could not be filled.

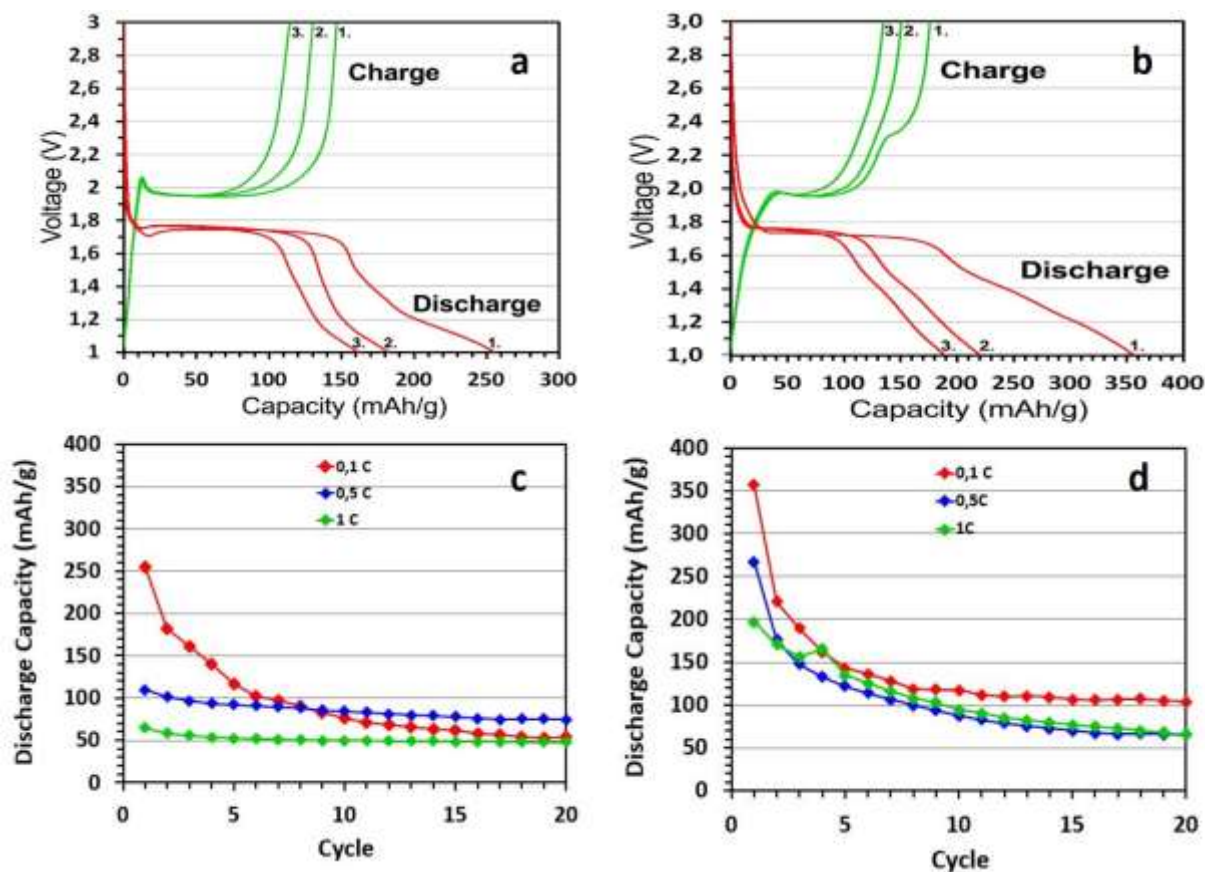


Figure 29. First three charge-discharge curves at 0.1C for a) Com, and b) SG and evolution of reversible capacity at different current rates over 20 cycles for c) Com, and d) SG

The discharge capacity of the Com and SG at different current rates was examined for 50 cycles. The current rates were increased for every ten cycles until the fortieth cycle then current rate was decreased back to its initial value (0.1C) for the last ten cycles. For the Com electrode (Fig. 30), at the first region (0.1 C), the discharge capacity dropped very fast and at the tenth cycle the capacity was 88 mAh/g. After increasing the current rate to 0.5 C, the capacity dropped almost to zero. This situation continued for 1 C and 5C until current rate decreased back to 0.1C. For a stable system, the capacity should have increased to a value close to 88 mAh/g. However the capacity increased 72 mAh/g and kept decreasing

until the end of 50 cycles. In the case of SG (Fig. 30), the drop of discharge capacity was not that high at the first region and at the tenth cycle it dropped to 119 mAh/g. Even though the performance at high current rates was not satisfactory it was better than Com. After reaching the last region, the capacity increased to 102 mAh/g and stayed constant during the last ten cycles. The recovery was better with minimal capacity loss, thus SG electrode is more stable than Com mainly due to its smaller particle size and higher surface area.

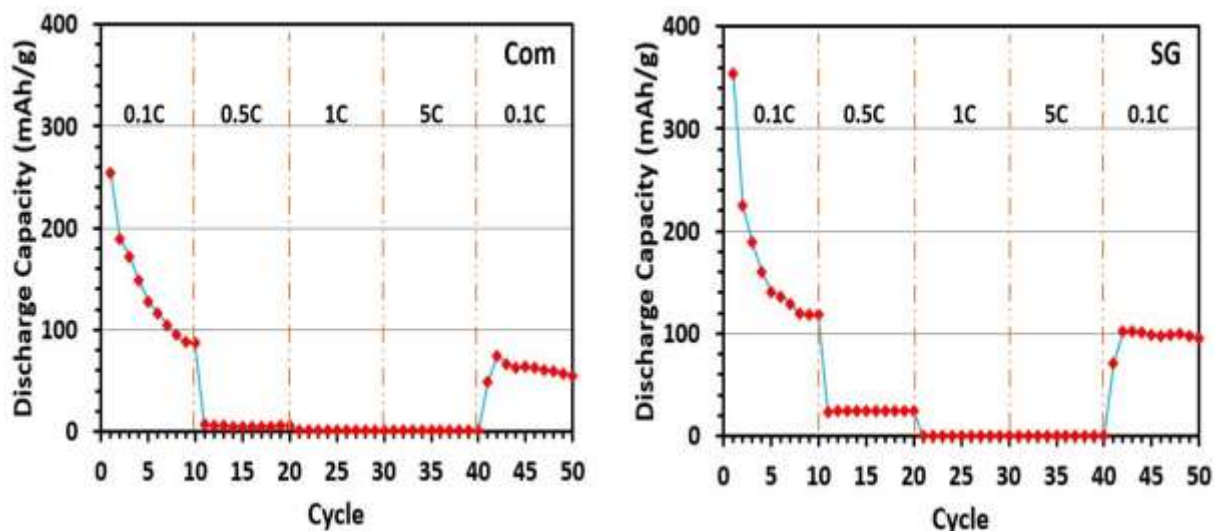


Figure 30. Rate capabilities of Com and SG

### 3.2. Structural and electrochemical properties for titanate samples

It is known that some Ti-O bonds of  $\text{TiO}_2$  are broken when they used as precursor treated hydrothermally with high concentrated NaOH [64]. This leads to forming layered titanate ( $\text{Na}_2\text{Ti}_3\text{O}_7$ ) then it is washed with an acidic solution and water. Washing step controls the amount of  $\text{Na}^+$  in the sample, then due to located imbalance  $\text{H}^+$  and  $\text{Na}^+$  between the layers, the surface energy of the layers increase and it force the layers to bend to form tubes [70]. Some researchers claim that acid washing is not a crucial step for nanotube formation and just during NaOH treatment that will be formed [63, 122]. While there are some other studies that clearly reported that acid washing affects the formation and structure of the final titanate nanotubes [64, 123]. Such differences in experimental finding are the result of differences in NaOH treatment conditions like temperature, duration applied, particle size

and whether the medium is mixed or not. Treatment with a concentrated NaOH at high temperature or long experimental durations might be leading to formation of titanate nanotubes [70, 99]. Another factor that might help to formation of nanotubes is agitation, it was reported that nanotubes were formed at 110 °C of NaOH treatment after 20 hours with agitation [122]. However, for the cases where after hydrothermal treatment only an intermediate structure is obtained due to low temperature and short experimental duration, acid washing step can help the formation of titanate nanotubes [64, 123].

In this study, SG and Com were treated with NaOH at 130 °C for 4 hours, then specimens were washed with solutions having different pH values to obtain titanates (the pH was adjusted using 0.1 M HCl). The samples that were obtained from SG or Com were coded with label that contains letters followed by a number. If the sample was hydrothermally treated with NaOH, then the label starts with the letter N. Then depending on the starting materials, after the letter N, S (for SG) or C (for Com) is used. The number is the pH value in which the sample was washed, for example if SG was used as starting material and that sample was washed at a pH of 4, then it was coded as NS4.

### 3.2.1. XRD characterization

Structural change of the samples hydrothermal treatment was first studied by XRD. According to Fig. 31a, which is XRD patterns of hydrothermal treated Com washed in different pH values (NC series), by decreasing the pH of the solutions, the structure changes from titanates to anatase, this can be imply from intensity titanates diffraction peaks positioned at  $2\theta = 11^\circ$ ,  $24^\circ$  and  $28^\circ$  associated with the (2 0 0), (1 0 1) and (3 0 0) planes of trititanate ( $\text{H}_2\text{Ti}_3\text{O}_7$  and  $\text{Na}_2\text{Ti}_3\text{O}_7$ ) (JCPDS no: 31-1329) that were decreasing and appearance of anatase diffraction peak at  $2\theta = 25.4^\circ$  due to  $\text{H}^+$  attack and restructuring  $\text{TiO}_6$  octahedral to form anatase [122]. This structure change can be also seen in the XRD patterns of hydrothermal treated SG (NS series) (Fig 31b).

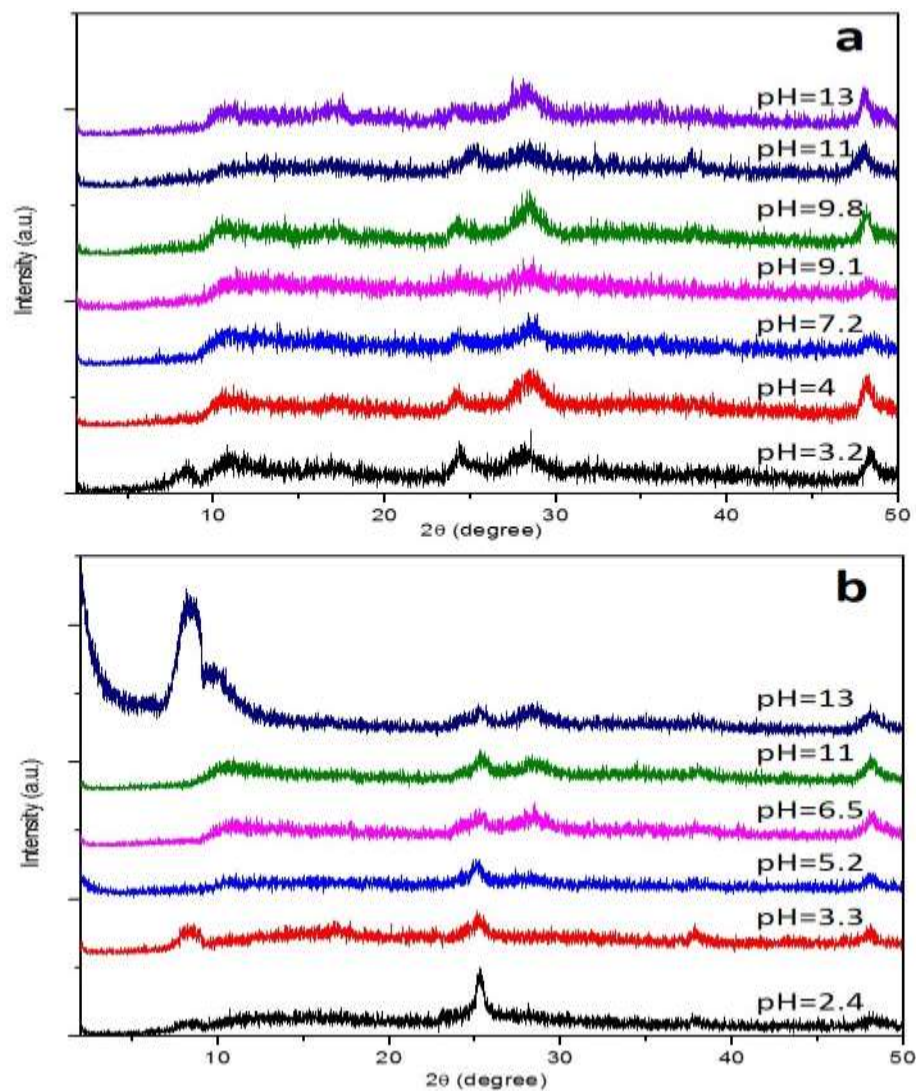


Figure 31. XRD patterns of titanates samples washed in solutions with different pH values.

(a) NC, (b) NS

### 3.2.2. SEM characterization

Study on the samples morphology reveals that nano structure of the sample is highly influenced by post-treatment step. By decreasing the pH values of the solution in which the samples were washed, the nanotubes size was decreased due to present more  $H^+$  rather than  $Na^+$  in the system which leads to decreasing Na/H ratio. At higher pH values, the materials has more  $Na^+$  than  $H^+$  thus at higher pH values the nanotubes should be thicker. Fig. 32 shows the SEM images of the NC samples with different post-treatment conditions, the diameters of the nanotubes in NC4, NC7.2, NC9.8 and NC11 are in the range of 15-20nm,

21-27nm, 25-30nm and 30-36nm, respectively. Some researchers obtained titanate nanotubes hydrothermally with anatase TiO<sub>2</sub> precursor at 130 °C and duration of 72 hours, they got 9nm nanotubes [102, 103]. Duration of the experiment make such a difference in nanotubes diameter.

Fig.33 shows the NS samples washed in solutions with different pH values, SEM images of NS2.4 and NS3.3 (Fig. 33 a,b) show particle like morphology, according to their XRD profiles (Fig. 31 b) it can be concluded that they are in anatase phase due to extreme pH values solutions where they were washed in, while for higher pH values samples, nanotubes can be easily seen (Fig. 33 c,d,e). The nanotubes diameters were decrease like NC samples when NS samples were washed with severe pH solution. These diameters for NS5.2, NS6.5 and NS13 were measured to be in the ranges of 25-30nm, 28-34nm and 30-40nm, respectively.

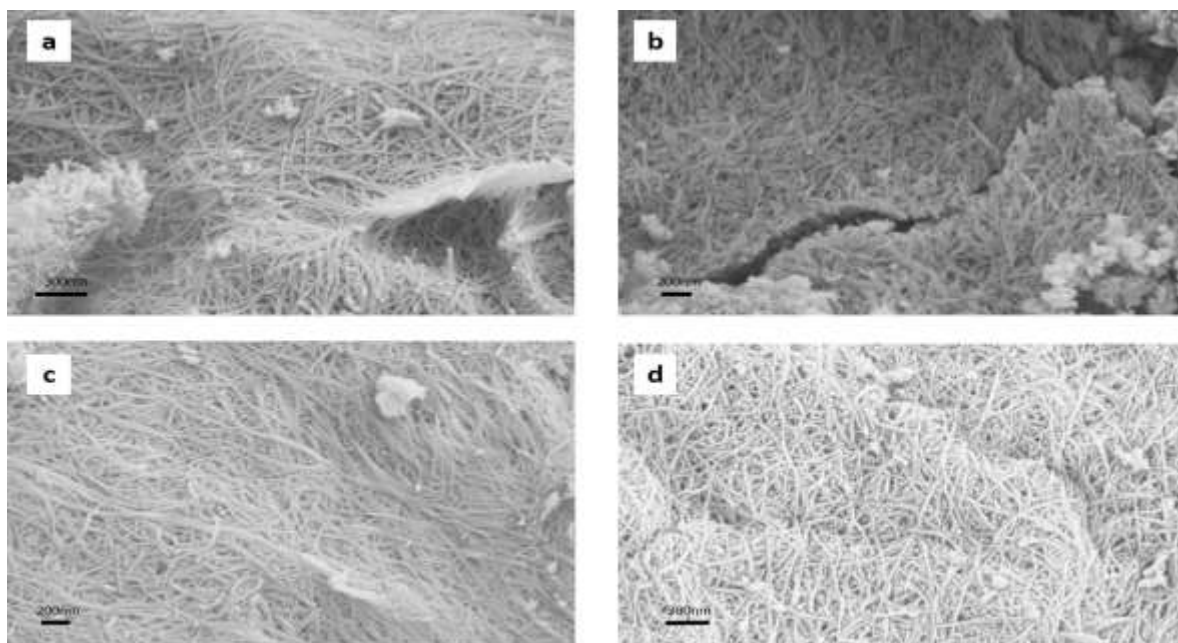


Figure 32. SEM images of NC samples with pH values of (a) 4, (b) 7.2, (c) 9.8 and (d) 11

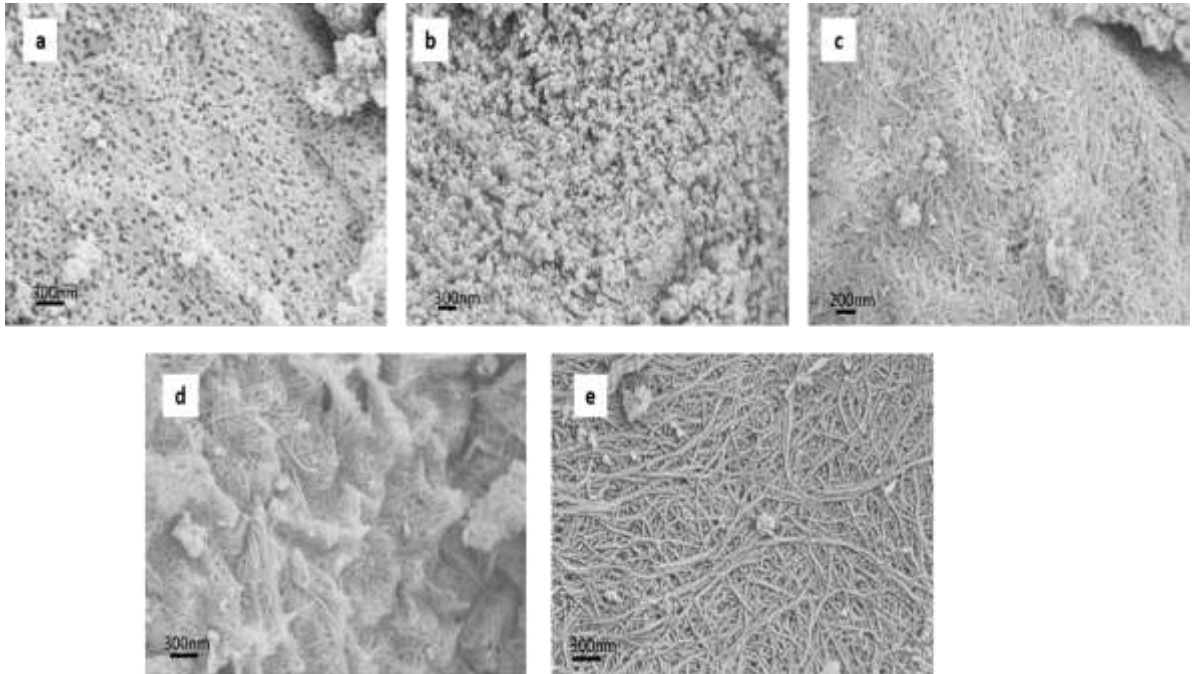


Figure 33. SEM images of NS samples with pH values of (a) 2.4, (b) 3.3, (c) 5.2, (d) 6.5 and (e) 13

### 3.2.3. Surface area and pore size analyses

Figure 34 shows the variations of surface area and interlayer distances with respect to pH for NC and NS samples. Surface area for both series of samples was increasing by decreasing the pH, in the NC series, NC4.5 has the highest surface area of 334 m<sup>2</sup>/g. while some researchers reported 195 m<sup>2</sup>/g [102] and 240 m<sup>2</sup>/g [104] surface areas for titanate nanotubes washed with water. It seems that highest surface area is belong to those samples that were washed at the pH range of 4-5. Getting far from this range towards higher pH values, the surface area will be decreased due to replacement Na<sup>+</sup> in the structure more than H<sup>+</sup>, while both series of samples showed wider interlayer distances at higher pH values due to store more Na<sup>+</sup> content between the layers than H<sup>+</sup>. By decreasing the pH values, interlayer distances were decreased.

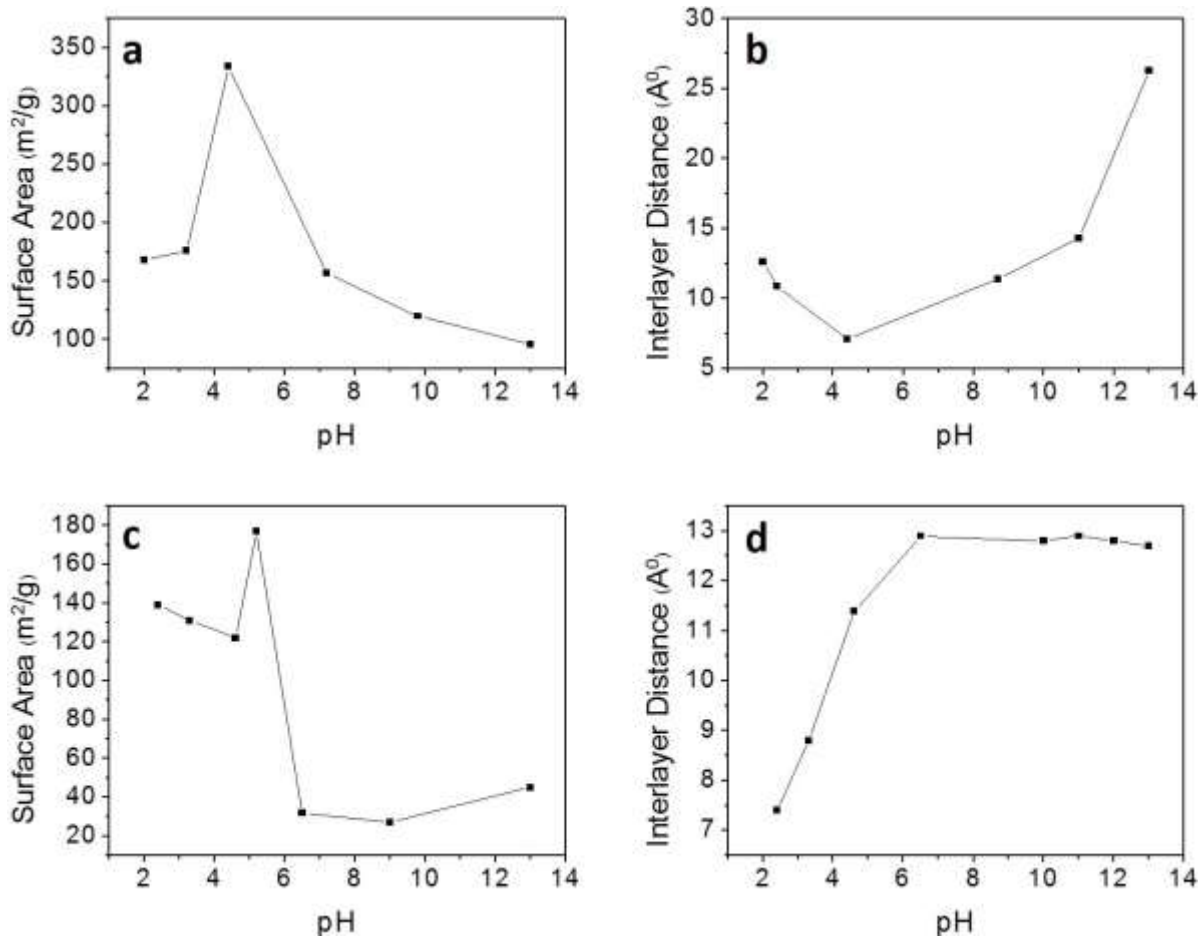


Figure 34. (a, b) NC samples a) surface area, b) interlayer distances, (c, d) NS samples c) surface area, d) interlayer distance

### 3.2.4. Electrochemical characterization

NC4 and NC9.8 have a pair of broad oxidation-reduction peaks in their CV patterns (Fig. 35) indication their pseudocapacitive behavior of this materials which occurs during hydrothermal treatment when they turned to titanate from anatase , surface area increased and form layered structure with pseudocapacitive behavior [124]. Due to multi-layered and tubular structure of these titanate nanotubes, Li<sup>+</sup> can easily intercalate and deintercalate to their structures. This can be resulted in broad oxidation-reduction peaks in their CV profiles [116].

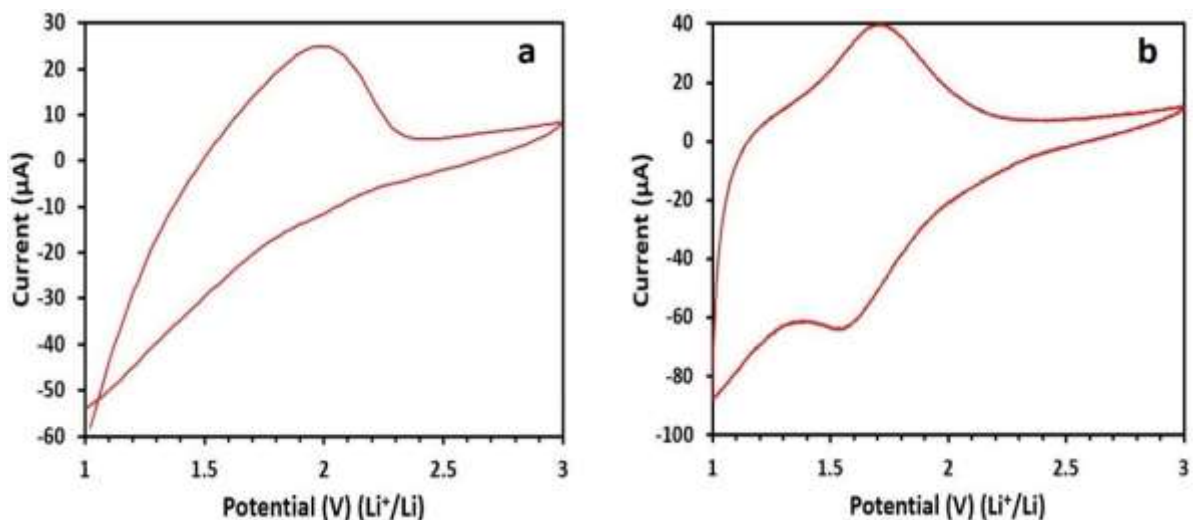


Figure 35. Cyclic voltammetry of a) NC4, and b) NC9.8

The first three charge-discharge profiles at current rate of 0.1C of NC4 and NC9.8 are shown in Fig 36 (a, b). It was shown that interlayer distances of NC9.8 is more than NC4 (Fig.34) also NC9.8 nanotubes is thicker than NC4 nanotubes (Fig. 32 a,c) thus this enhancement in interlayer distances and nanotubes diameters provide more free space for  $\text{Li}^+$  to intercalate to NC9.8 lattice, which can be resulted in more initial discharge capacity for NC9.8. This capacity for NC9.8 is 980 mAh/g, while it is 823 mAh/g for NC4, which is still high enough due to its high surface area ( $130.6 \text{ m}^2/\text{g}$ ). Some studies reported initial discharge capacity of 182 mAh/g at 0.48C [77] and 330 mAh/g at 0.3C [74] for titanate nanotubes, while we obtain higher initial discharge capacity even at higher current rate (0.5C), 365 mAh/g for NC4 and 385 mAh/g for NC9.8. However capacity fading occurs for both of them in the beginning of charge-discharge cycles due to trapping some  $\text{Li}^+$  in the lattice [124], consequently losing their capacities is followed. The capacity reversibility of the samples was examined at different current rates in 20 cycles (Fig 36 d, e). NC4 shows 104 mAh/g as reversible capacity at 0.1C after 20 cycles, while NC9.8 with wider interlayer distances has 131 mAh/g reversible capacity after 20 cycles at 0.1C due to less trapped  $\text{Li}^+$  in NC9.8 lattice.

M. Eom and his co-workers reported that reversible capacity of titanate nanotubes is highly affected by interlayer spacing, they enlarged the interlayer spacing of titanate by treating

titanate with one of the Li, Na and K alkali solutions to exchange ions among layers. They obtained 230 mAh/g initial discharge capacity at 0.1C for sodium titanate nanotubes [125] thus it can be seen that our titanate nanotubes were significantly modified.

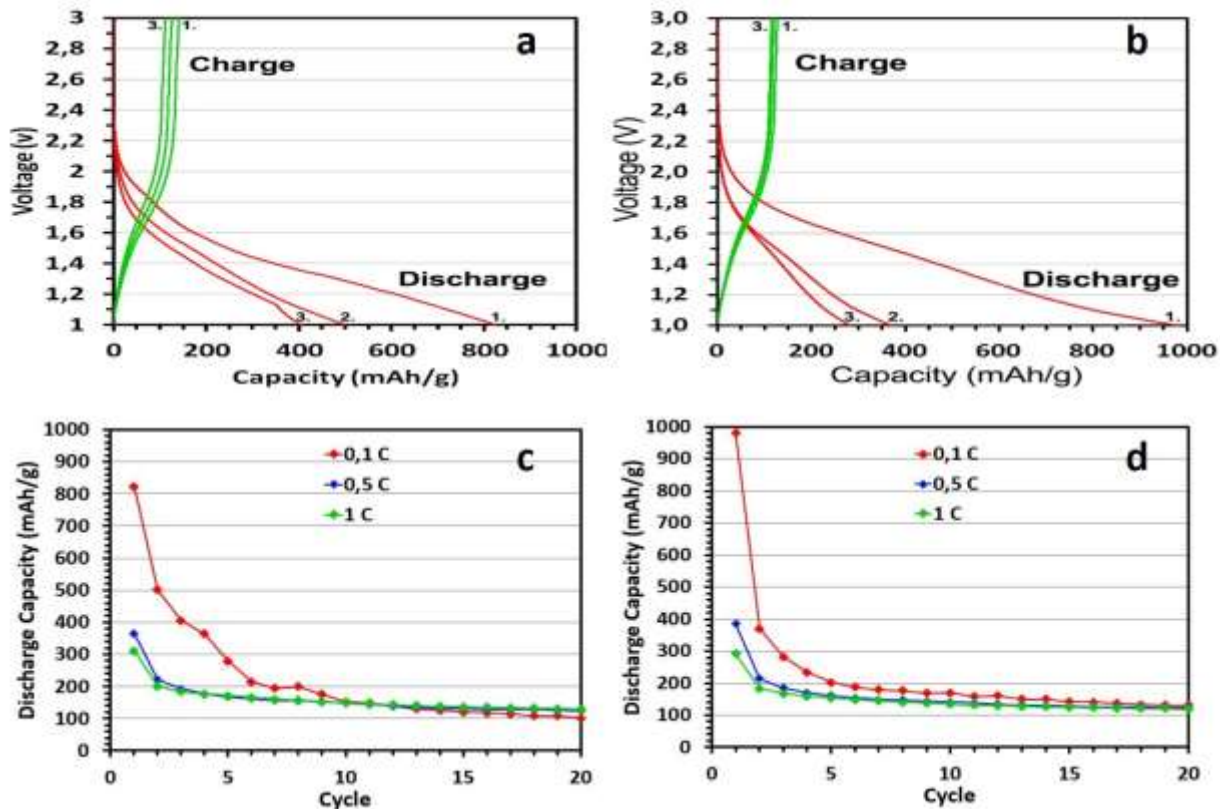


Figure 36. First three charge-discharge curves at 0.1C for NC samples washed in pH value of a) 4, and b) 9.8, and evolution of reversible capacity at different current rates in 20 cycles for c) NC4, and d) NC9.8

Rate capabilities of NC4 and NC9.8 samples is shown in Fig. 37. For NC4, the discharge capacity was decreased from 823 mAh/g to 151 mAh/g during first ten cycles at the current rate of 0.1C, then the current rate was increased to 0.5C, 1C and 5C for each ten cycles till fortieth cycle. In this three ten cycles, discharge capacity retention was observed. In the last ten cycles the current rate was return it its initial value (0.1C), and discharge capacity of 134 mAh/g was obtained for forty-first cycles and it was decreased to 102 mAh/g for fortieth cycle. For NC9.8 sample, this procedure took placed and discharge capacity of

tenth cycle, forty-first cycle and fiftieth cycle was 170 mAh/g, 157 mAh/g and 131 mAh/g, respectively. Titanate nanotubes showed excellent rate capability especially at wider interlayer distances, even at higher current rate irreversible capacity is negligible this is because of wide interlayer distances that provide enough space for  $\text{Li}^+$  to intercalate and deintercalate.

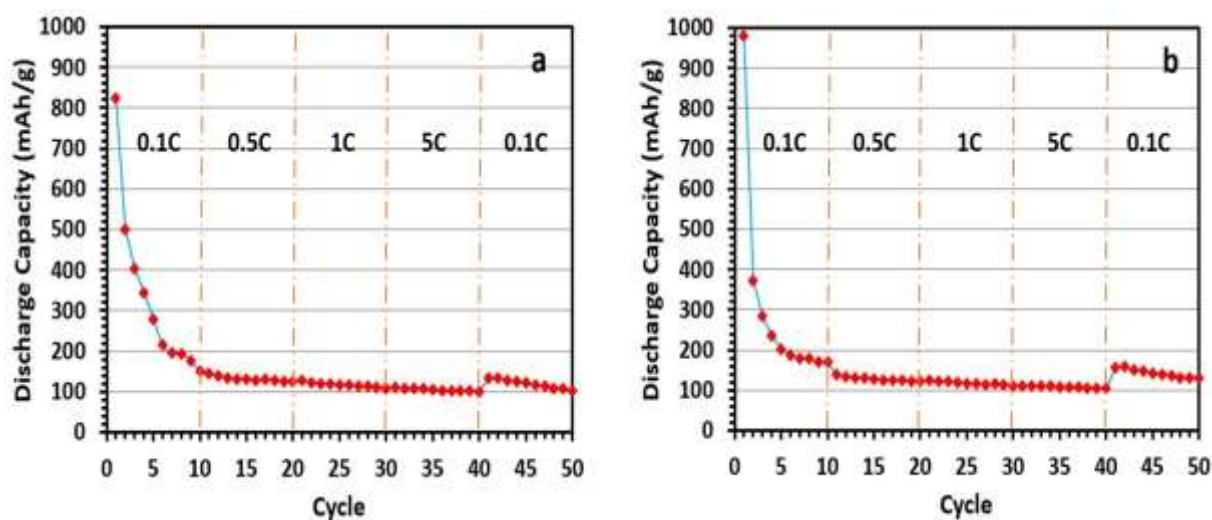


Figure 37. Rate capabilities of a) NC4, and b) NC9.8

It was reported that electrochemical properties are significantly affected by morphological characteristics of titanate nanotubes like surface area, nanotubes diameter and interlayer distances thus if these parameters will be improved then better electrochemical performance is followed.

### 3.3. Structural characterization of surfactant treated titanates

Titanate nanotubes with different post-treatment conditions were treated with dodecylamine ( $\text{C}_{12}\text{H}_{27}\text{N}$ )(surfactant) hydrothermally to replace  $\text{H}^+$  or  $\text{Na}^+$  with surfactant chains in order to modify the interlayer distances which has great impact on the electrochemical performance. It was reported that surface of titanate nanotubes has a point of zero charge ( $\text{pH}_{\text{PZC}}$ ) value of about 3.5 indicating that above this point the surface of titanate nanotubes

is negatively charged and by increasing the pH, the surface get more negatively charged [126, 127]. Thus during surfactant treatment, positive charged surfactant can easily enter electrostatically to titanate interlayers that were washed at pH values above 3.5. Surfactant treated samples are coded like hydrothermal treatment method. For example if NC4 was treated with surfactant, it was coded as SNC4.

### 3.3.1. XRD characterization

XRD profiles of surfactant treated NC (Fig. 38 a) and NS (Fig. 38 b) show that titanate diffraction peak at  $2\theta = 11^\circ$  corresponding to (2 0 0) plane, got intense indicating the presence of large surfactant cations between the layers and also this peak was shifted to lower angles revealing an increase in interlayer distances. This happened for both SNC and SNS series samples. In order to know how much the interlayer distances were increased, bragg's law was used to find the d-spacing of (2 0 0) plane of titanate nanotubes before and after surfactant treatment. It was calculated that d-spacing of the layer corresponding to peak at  $2\theta = 11^\circ$  for titanate before the surfactant treatment was 7 Å and after the surfactant treatment this value reached to 11 Å.

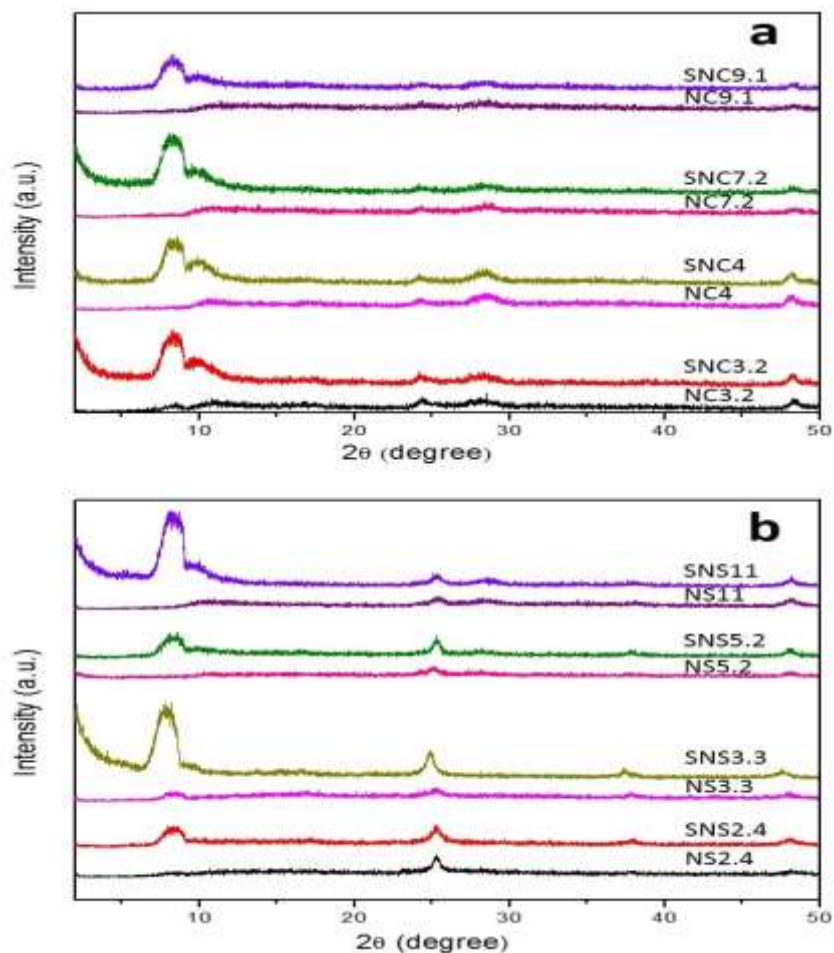


Figure 38. Comparison between XRD patterns of a) NC and SNC samples, and b) NS and SNS samples

### 3.3.2. SEM and TEM characterization

Fig. 39 shows the SEM images of some samples before and after surfactant treatment. Nanotubular structure of titanate was preserved after surfactant treatment while nanotubes become thicker. For NC4 sample, after surfactant treatment, the diameter of nanotubes increased from 15-20 nm to 35-55nm (Fig. 39a, b). This was also observed for NS samples, after surfactant treatment, NS5.2 nanotubes' diameter increased 25-30 nm to 40-60 nm (Fig. 39c, d). From TEM images for NC4.4, the average diameter of the nanotubes was measured as 9 nm. On the other hand, when this sample was treated with the surfactant the diameter increased to an average value of 14 nm (Fig. 40)

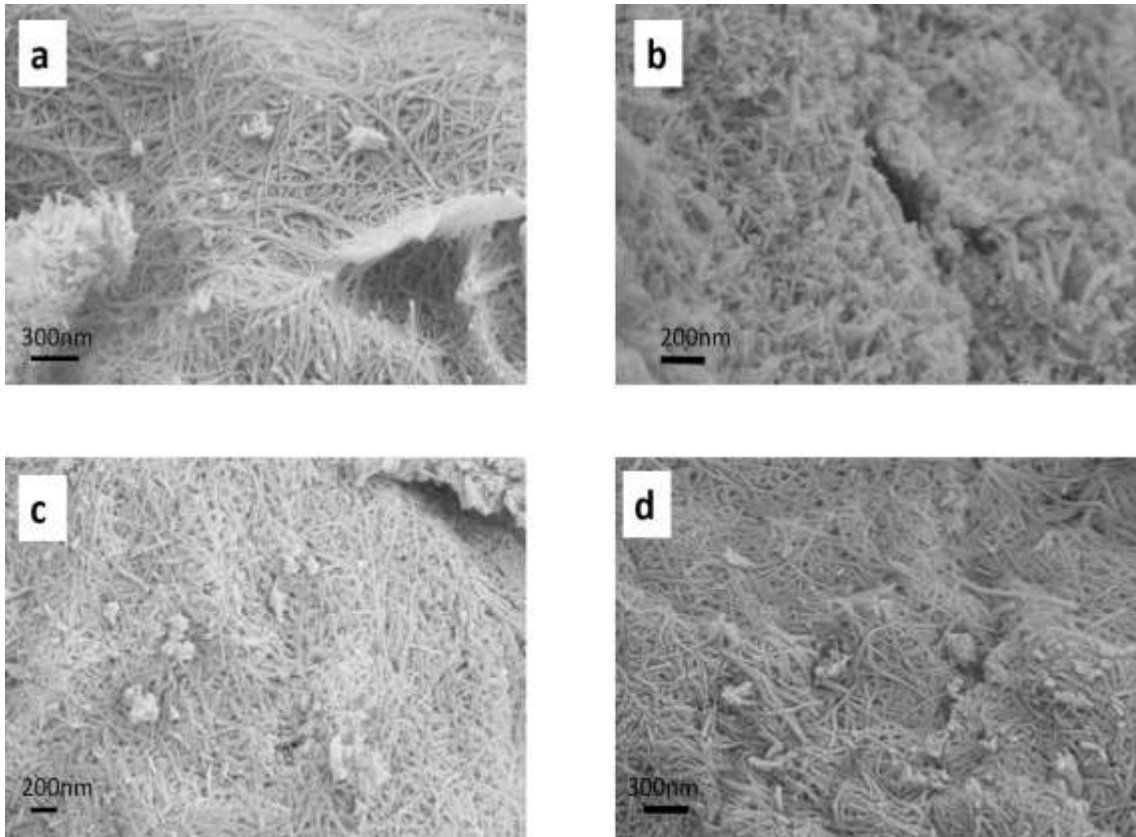


Figure 39. SEM images of a) NC4, b) SNC4, c) NS5.2, and d) SNS5.2

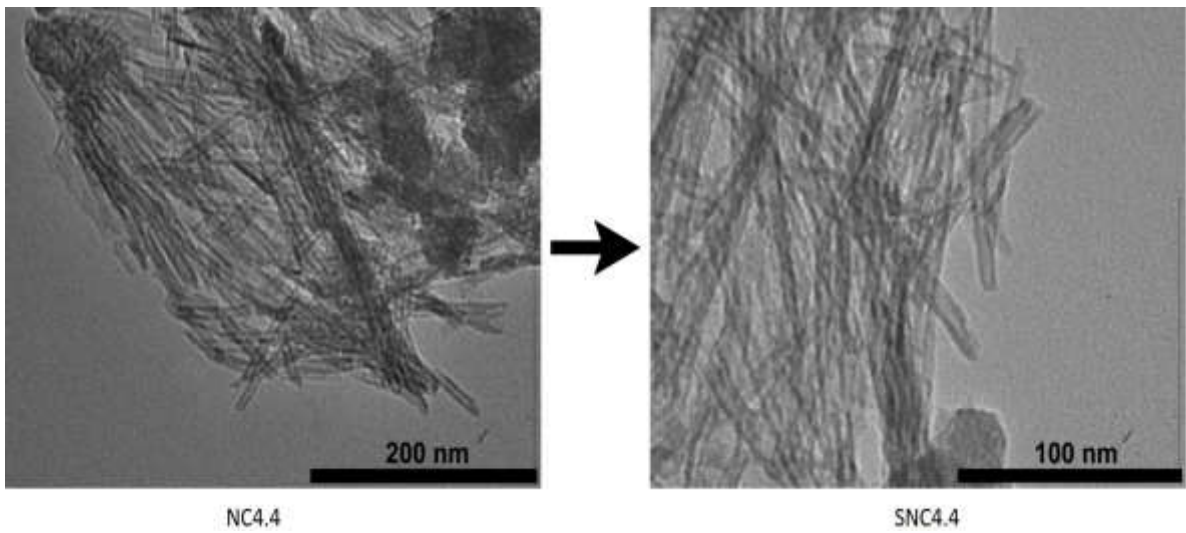


Figure 40. TEM images of NC4.4 and SNC4.4

### 3.3.3. Surface area and pore size analyses

BET and BJH analyses were made on surfactant treated NC and NS samples to determine surface area and interlayer distances. Fig.41 shows the effect of surfactant treatment on surface area and interlayer distances of titanates. It was indicated that during surfactant treatment, surface area of the titanates was decreased because surfactant cations were replaced with  $H^+$  or  $Na^+$  and it filled the pores in the structure leading to decreasing in surface area (Fig. 41 a, b), however the interlayer distances of the titanates was increased due to a force by surfactant cations on layers to be enlarged when they inserted to titanate lattice (Fig. 41 c, d). Both SNC and SNS samples were followed this procedure. The higher interlayer distance for SNC samples is  $21 \text{ \AA}$ , which is for SNC11. XRD profiles of surfactant treated NC (Fig. 38 a) and NS (Fig. 38 b) also support the BET results. The peak at  $2\theta = 11$  for titanates was shifted to lower degrees after surfactant treatment as the results of an increase in the interlayer distances. Also this peak got intense because surfactant cations filled the pores, as a consequence surface area was decreased.

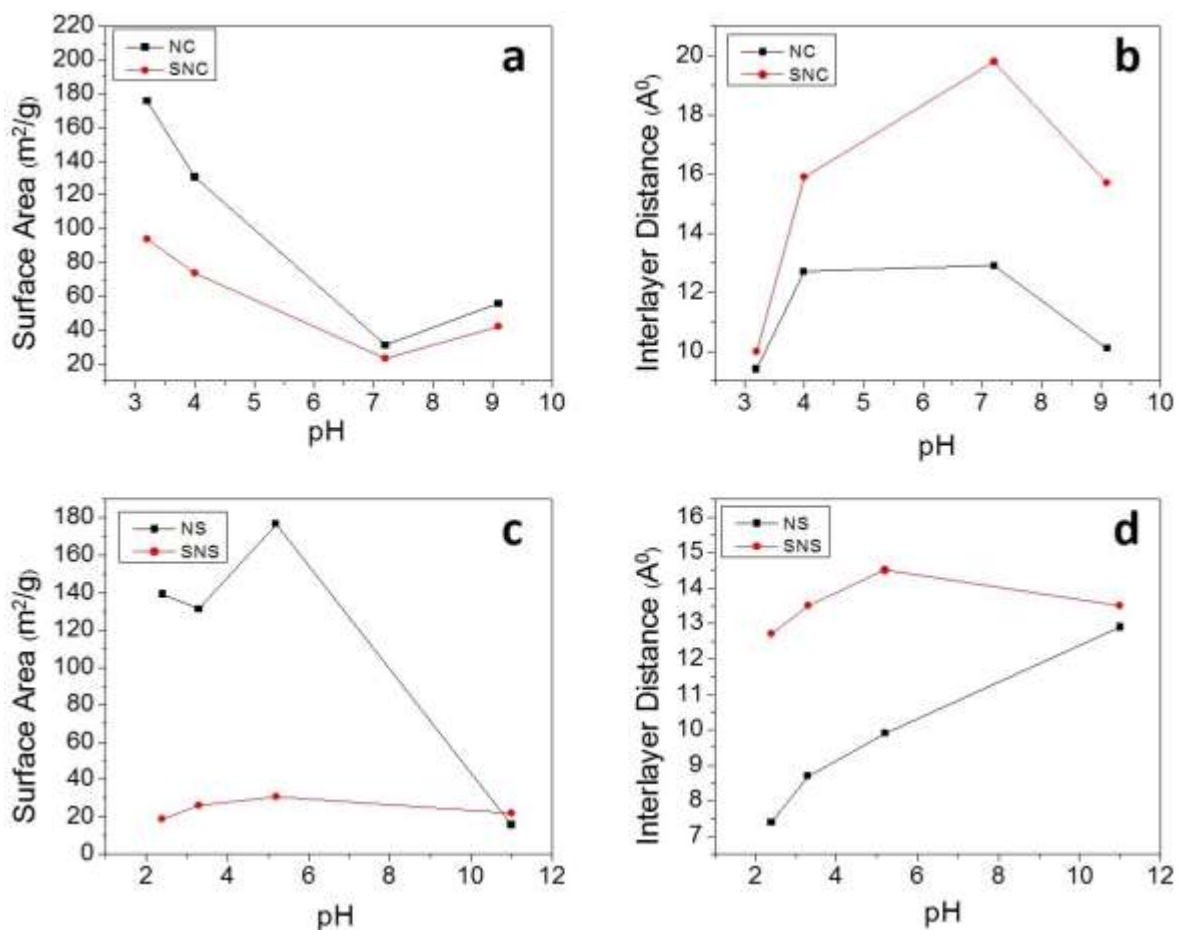


Figure 41. Comparison of a) surface area of NC and SNC samples, b) interlayer distances of NC and SNC samples, c) surface area of NS and SNS samples and d) interlayer distances of NS and SNS samples

### 3.3.4. Electrochemical characterization

In order to know the effect of surfactant on electrochemical performance of titanate nanotubes, we compared discharge capacity of NC4.4 and SNC4.4 at current rate of 0.1C for 19 cycles. As it was expected the initial discharge capacity of SNC4.4 (1232 mAh/g) is much higher than initial discharge capacity of NC4.4 (730 mAh/g) due to wider interlayer distances for SNC4.4 where Li<sup>+</sup> can be stored more and have more mobility. The discharge capacity was faded due to trapping Li<sup>+</sup> in the lattice but as it can be seen (Fig. 42) SNC4.4 shows better stability than NC4.4, again due to higher interlayer distances for SNC4.4.

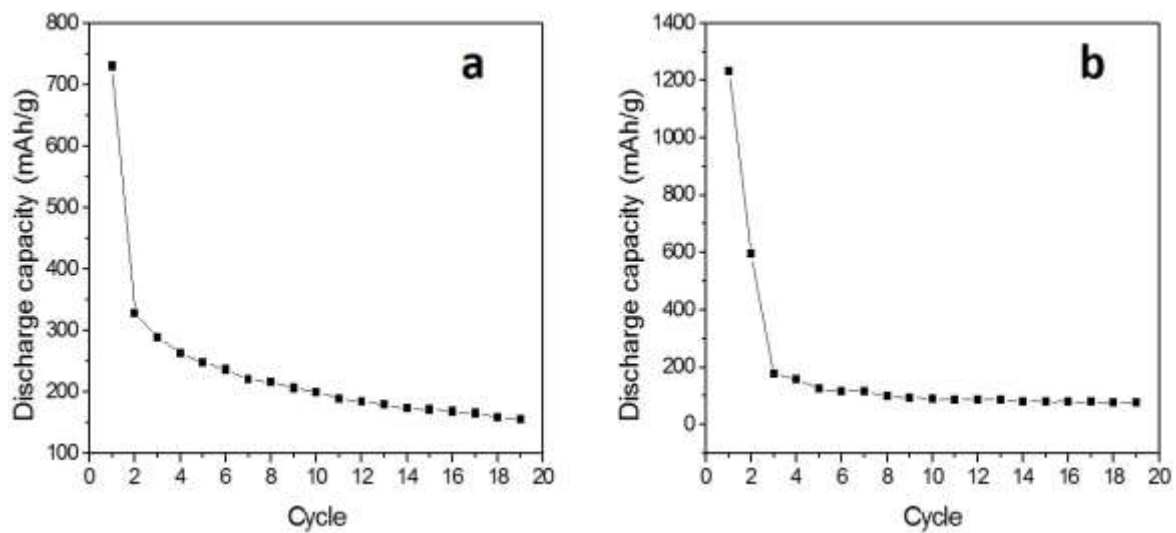


Figure 42. Discharge capacity of a) NC4.4, and b) SNC4.4 at 0.1C in 19 cycles

#### 4. Conclusion

In this study, anatase TiO<sub>2</sub> nanoparticles were prepared via sol-gel method. Moreover, as-prepared and commercial anatase were used as the precursors to synthesize titanate nanotubes hydrothermally in alkali conditions. Titanates interlayer distances were modified by a post-treatment step in which titanate were washed with solutions having different pH values. Furthermore, titanate nanotubes were treated with surfactants to expand the nanotubes. After that, structural and electrochemical characterizations were performed.

Anatase TiO<sub>2</sub> nanoparticles were successfully synthesized by sol-gel method with average particle size of 20nm and 63 m<sup>2</sup>/g surface area. While as-prepared TiO<sub>2</sub> anode showed 357 mAh/g initial discharge capacity at 0.1C current rate, the capacity of commercial TiO<sub>2</sub> anode was 256 mAh/g at 0.1C current rate. Smaller particle size and higher surface area of the sol-gel TiO<sub>2</sub> than the commercial one provided better electrochemical performance.

Titanate nanotubes were synthesized hydrothermally in high yields. By decreasing the pH value of the washing solution, the nanotube diameter decreased and after pH of 3 the titanates were converted back to anatase. The highest surface area was obtained at pH of 4.4 (334 m<sup>2</sup>/g) for hydrothermal treated commercial TiO<sub>2</sub> and getting away from this point to higher and lower pH values lead lower surface area values. The highest interlayer distances was observed at pH of 13 (26 Å) for hydrothermal treated commercial TiO<sub>2</sub>. Titanates showed exceptional rate capabilities especially at wider interlayer distances. High specific capacity of 980 mAh/g was observed for titanate at pH of 9.8 due to its large interlayer distance.

Nanotubes diameter, surface area and interlayer distances of titanates were significantly affected by surfactant treatment. Surfactant treated titanates showed thicker nanotubes, lower surface area and higher interlayer distances than titanates without surfactant treatment. Moreover, a much higher discharge capacity of 1232 mAh/g was obtained due to having expanded titanate nanotubes.

## References

1. Crossette, B. *The state of world population 2011*. Version 2011; Available from: [www.unfpa.org](http://www.unfpa.org).
2. TOLLEFSON, #160, and Jeff, *CHARGING UP THE FUTURE*. Vol. 456. 2008, London, ROYAUME-UNI: Nature Publishing Group. 5.
3. Scrosati, B. and J. Garche, *Lithium batteries: Status, prospects and future*. Journal of Power Sources, 2010. **195**(9): p. 2419-2430.
4. *Nickel Metal Hydride Batteries*. Available from: <http://www.mpoweruk.com/nimh.htm>.
5. Soria, M.L., J. Chacón, and J.C. Hernández, *Metal hydride electrodes and Ni/MH batteries for automotive high power applications*. Journal of Power Sources, 2001. **102**(1–2): p. 97-104.
6. Nishi, Y., *Lithium ion secondary batteries; past 10 years and the future*. Journal of Power Sources, 2001. **100**(1–2): p. 101-106.
7. Buchmann, I. 2013; Available from: [www.batteryuniversity.com](http://www.batteryuniversity.com).
8. Yoshino, A., *The Birth of the Lithium-Ion Battery*. Angewandte Chemie International Edition, 2012. **51**(24): p. 5798-5800.
9. Landi, B.J., et al., *Carbon nanotubes for lithium ion batteries*. Energy & Environmental Science, 2009. **2**(6): p. 638-654.
10. Mizushima, K., et al., *Li<sub>x</sub>CoO<sub>2</sub> (0 < x ≤ 1): A new cathode material for batteries of high energy density*. Solid State Ionics, 1981. **3–4**(0): p. 171-174.
11. *Battery Technologies and Markets*.
12. Doh, C.-H., et al., *Thermal and electrochemical behaviour of C/Li<sub>x</sub>CoO<sub>2</sub> cell during safety test*. Journal of Power Sources, 2008. **175**(2): p. 881-885.
13. Cho, J., Y.J. Kim, and B. Park, *Novel LiCoO<sub>2</sub> Cathode Material with Al<sub>2</sub>O<sub>3</sub> Coating for a Li Ion Cell*. Chemistry of Materials, 2000. **12**(12): p. 3788-3791.
14. Sixu, D., et al., *Research Progress in Improving the Rate Performance of LiFePO<sub>4</sub> Cathode Materials*. Nano-Micro Letters, 2014. **6**(3).
15. Lee, S., et al., *Carbon-Coated Single-Crystal LiMn<sub>2</sub>O<sub>4</sub> Nanoparticle Clusters as Cathode Material for High-Energy and High-Power Lithium-Ion Batteries*. Angewandte Chemie International Edition, 2012. **51**(35): p. 8748-8752.
16. Gao, Y., J.N. Reimers, and J.R. Dahn, *Changes in the voltage profile of Li/Li<sub>1+x</sub>Mn<sub>2-x</sub>O<sub>4</sub> cells as a function of x*. Physical Review B, 1996. **54**(6): p. 3878-3883.
17. Palacin, M.R., *Recent advances in rechargeable battery materials: a chemist's perspective*. Chemical Society Reviews, 2009. **38**(9): p. 2565-2575.
18. Szczech, J.R. and S. Jin, *Nanostructured silicon for high capacity lithium battery anodes*. Energy & Environmental Science, 2011. **4**(1): p. 56-72.
19. Cabana, J., et al., *Beyond Intercalation-Based Li-Ion Batteries: The State of the Art and Challenges of Electrode Materials Reacting Through Conversion Reactions*. Advanced Materials, 2010. **22**(35): p. E170-E192.
20. Xu, J.S. and Y.J. Zhu, *Monodisperse Fe<sub>3</sub>O<sub>4</sub> and γ-Fe<sub>2</sub>O<sub>3</sub> magnetic mesoporous microspheres as anode materials for lithium-ion batteries*. ACS Applied Materials and Interfaces, 2012. **4**(9): p. 4752-4757.
21. Kang, N., et al., *Nanoparticulate iron oxide tubes from microporous organic nanotubes as stable anode materials for lithium ion batteries*. Angewandte Chemie - International Edition, 2012. **51**(27): p. 6626-6630.

22. Mitra, S., et al., *Growth and electrochemical characterization versus lithium of Fe 3O4 electrodes made via electrodeposition*. *Advanced Functional Materials*, 2006. **16**(17): p. 2281-2287.
23. Wu, H. and Y. Cui, *Designing nanostructured Si anodes for high energy lithium ion batteries*. *Nano Today*, 2012. **7**(5): p. 414-429.
24. Schauerman, C.M., et al., *Recycling single-wall carbon nanotube anodes from lithium ion batteries*. *Journal of Materials Chemistry*, 2012. **22**(24): p. 12008-12015.
25. Frackowiak, E. and F. Béguin, *Electrochemical storage of energy in carbon nanotubes and nanostructured carbons*. *Carbon*, 2002. **40**(10): p. 1775-1787.
26. Su, F.-Y., et al., *Could graphene construct an effective conducting network in a high-power lithium ion battery?* *Nano Energy*, 2012. **1**(3): p. 429-439.
27. Yoo, E., et al., *Large Reversible Li Storage of Graphene Nanosheet Families for Use in Rechargeable Lithium Ion Batteries*. *Nano Letters*, 2008. **8**(8): p. 2277-2282.
28. Kim, C., et al., *Fabrication of Electrospinning-Derived Carbon Nanofiber Webs for the Anode Material of Lithium-Ion Secondary Batteries*. *Advanced Functional Materials*, 2006. **16**(18): p. 2393-2397.
29. Lee, S.W., et al., *High-power lithium batteries from functionalized carbon-nanotube electrodes*. *Nat Nano*, 2010. **5**(7): p. 531-537.
30. Kaskhedikar, N.A. and J. Maier, *Lithium storage in carbon nanostructures*. *Advanced Materials*, 2009. **21**(25-26): p. 2664-2680.
31. Orsini, F., et al., *In situ SEM study of the interfaces in plastic lithium cells*. *Journal of Power Sources*, 1999. **81-82**(0): p. 918-921.
32. Tarascon, J.M. and M. Armand, *Issues and challenges facing rechargeable lithium batteries*. *Nature*, 2001. **414**(6861): p. 359-367.
33. Xu, K., *Nonaqueous Liquid Electrolytes for Lithium-Based Rechargeable Batteries*. *Chemical Reviews*, 2004. **104**(10): p. 4303-4418.
34. Pinson, M.B. and M.Z. Bazant, *Theory of SEI Formation in Rechargeable Batteries: Capacity Fade, Accelerated Aging and Lifetime Prediction*. *Journal of The Electrochemical Society*, 2013. **160**(2): p. A243-A250.
35. Atwater, M., *Engineers find new possibilities for Li-ion batteries by taking a "deeper" look*. 2013.
36. Winter, M. and R.J. Brodd, *What are batteries, fuel cells, and supercapacitors?* *Chem Rev*, 2004. **104**(10): p. 4245-69.
37. Goriparti, S., et al., *Review on recent progress of nanostructured anode materials for Li-ion batteries*. *Journal of Power Sources*, 2014. **257**: p. 421-443.
38. Lin, H., et al., *Size dependency of nanocrystalline TiO2 on its optical property and photocatalytic reactivity exemplified by 2-chlorophenol*. *Applied Catalysis B: Environmental*, 2006. **68**(1-2): p. 1-11.
39. Lusvardi, V.S., et al., *An NEXAFS investigation of the reduction and reoxidation of TiO2(001)*. *Surface Science*, 1998. **397**(1-3): p. 237-250.
40. Sherrill, A.B., et al., *NEXAFS investigations of cyclooctatetraene on TiO2(001)*. *Surface Science*, 2001. **492**(3): p. 203-213.
41. Fujishima, A., X. Zhang, and D.A. Tryk, *TiO2 photocatalysis and related surface phenomena*. *Surf. Sci. Rep.*, 2008. **63**(12): p. 515-582.
42. Chen, X. and S.S. Mao, *Titanium Dioxide Nanomaterials: Synthesis, Properties, Modifications, and Applications*. *Chem. Rev. (Washington, DC, U. S.)*, 2007. **107**(7): p. 2891-2959.

43. Kavan, L., et al., *Electrochemical and photoelectrochemical investigation of single-crystal anatase*. Journal of the American Chemical Society, 1996. **118**(28): p. 6716-6723.
44. Banfield, J.F. and D.R. Veblen, *Conversion of perovskite to anatase and TiO<sub>2</sub> (B): a TEM study and the use of fundamental building blocks for understanding relationships among the TiO<sub>2</sub> minerals*. American Mineralogist, 1992. **77**(5-6): p. 545-557.
45. *Jade Database*.
46. Sudant, G., et al., *Electrochemical lithium reactivity with nanotextured anatase-type TiO<sub>2</sub>*. Journal of Materials Chemistry, 2005. **15**(12): p. 1263-1269.
47. Baddour-Hadjean, R., et al., *Raman investigation of the structural changes in anatase Li<sub>x</sub>TiO<sub>2</sub> upon electrochemical lithium insertion*. Journal of Raman Spectroscopy, 2004. **35**(7): p. 577-585.
48. Kim, J. and J. Cho, *Rate characteristics of anatase TiO<sub>2</sub> nanotubes and nanorods for lithium battery anode materials at room temperature*. Journal of the Electrochemical Society, 2007. **154**(6): p. A542-A546.
49. Park, S.J., Y.J. Kim, and H. Lee, *Synthesis of carbon-coated TiO<sub>2</sub> nanotubes for high-power lithium-ion batteries*. Journal of Power Sources, 2011. **196**(11): p. 5133-5137.
50. Yurum, A., *The synthesis of titanium dioxide photocatalysts by sol-gel method : the effect of hydrotherman treatment conditions and use of carbon nanotube template*. 2009.
51. Yang, Z., et al., *Nanostructures and lithium electrochemical reactivity of lithium titanites and titanium oxides: A review*. Journal of Power Sources, 2009. **192**(2): p. 588-598.
52. Koudriachova, M.V., N.M. Harrison, and S.W. De Leeuw, *Effect of diffusion on Lithium intercalation in titanium dioxide*. Physical Review Letters, 2001. **86**(7): p. 1275-1278.
53. Stashans, A., et al., *Theoretical study of lithium intercalation in rutile and anatase*. Physical Review B - Condensed Matter and Materials Physics, 1996. **53**(1): p. 159-170.
54. Baudrin, E., et al., *Structural evolution during the reaction of Li with nano-sized rutile type TiO<sub>2</sub> at room temperature*. Electrochemistry Communications, 2007. **9**(2): p. 337-342.
55. Jiang, C., et al., *Nanocrystalline Rutile TiO<sub>2</sub> Electrode for High-Capacity and High-Rate Lithium Storage*. Electrochemical and Solid-State Letters, 2007. **10**(5): p. A127-A129.
56. Wagemaker, M., et al., *Multiple Li positions inside oxygen octahedra in lithiated TiO<sub>2</sub> anatase*. Journal of the American Chemical Society, 2003. **125**(3): p. 840-848.
57. Marchand, R., L. Brohan, and M. Tournoux, *TiO<sub>2</sub>(B) a new form of titanium dioxide and the potassium octatitanate K<sub>2</sub>Ti<sub>8</sub>O<sub>17</sub>*. Materials Research Bulletin, 1980. **15**(8): p. 1129-1133.
58. Armstrong, A.R., et al., *Lithium-ion intercalation into TiO<sub>2</sub>-B nanowires*. Advanced Materials, 2005. **17**(7): p. 862-865.
59. Armstrong, A.R., et al., *TiO<sub>2</sub>-B nanowires*. Angewandte Chemie - International Edition, 2004. **43**(17): p. 2286-2288.
60. Saponjic, Z.V., et al., *Shaping Nanometer-Scale Architecture Through Surface Chemistry*. Advanced Materials, 2005. **17**(8): p. 965-971.
61. Dimitrijevic, N.M., et al., *Assembly and Charge Transfer in Hybrid TiO<sub>2</sub> Architectures Using Biotin-Avidin as a Connector*. Journal of the American Chemical Society, 2005. **127**(5): p. 1344-1345.
62. Joo, J., et al., *Large-Scale Synthesis of TiO<sub>2</sub> Nanorods via Nonhydrolytic Sol-Gel Ester Elimination Reaction and Their Application to Photocatalytic Inactivation of E. coli*. The Journal of Physical Chemistry B, 2005. **109**(32): p. 15297-15302.
63. Du, G.H., et al., *Preparation and structure analysis of titanium oxide nanotubes*. Appl. Phys. Lett., 2001. **79**(22): p. 3702-3704.
64. Kasuga, T., et al., *Titania nanotubes prepared by chemical processing*. Adv. Mater. (Weinheim, Ger.), 1999. **11**(15): p. 1307-1311.

65. Liu, G., J. Qu, and H. Wang, *Morphology-control synthesis and electrochemical performance of titanate and anatase TiO<sub>2</sub>*. Journal of Alloys and Compounds, 2013. **578**: p. 345-348.
66. Lim, S.H., et al., *Room-temperature hydrogen uptake by TiO<sub>2</sub> nanotubes*. Inorganic Chemistry, 2005. **44**(12): p. 4124-4126.
67. Wang, D., et al., *Synthesis and characterization of anatase TiO<sub>2</sub> nanotubes with uniform diameter from titanium powder*. Materials Letters, 2008. **62**(12-13): p. 1819-1822.
68. Peng, H., G. Li, and Z. Zhang, *Synthesis of bundle-like structure of titania nanotubes*. Materials Letters, 2005. **59**(10): p. 1142-1145.
69. Nakahira, A., T. Kubo, and C. Numako, *Formation mechanism of TiO<sub>2</sub>-derived titanate nanotubes prepared by the hydrothermal process*. Inorganic Chemistry, 2010. **49**(13): p. 5845-5852.
70. Zhang, S., et al., *Formation mechanism of H<sub>2</sub>Ti<sub>3</sub>O<sub>7</sub> nanotubes*. Phys Rev Lett, 2003. **91**(25): p. 256103.
71. Kasuga, T., et al., *Formation of titanium oxide nanotube*. Langmuir, 1998. **14**(12): p. 3160-3163.
72. Eguia-Barrio, A., et al., *Structure of H<sub>2</sub>Ti<sub>3</sub>O<sub>7</sub> and its evolution during sodium insertion as anode for Na ion batteries*. Phys Chem Chem Phys, 2015. **17**(10): p. 6988-94.
73. Augustyn, V., P. Simon, and B. Dunn, *Pseudocapacitive oxide materials for high-rate electrochemical energy storage*. Energy & Environmental Science, 2014. **7**(5): p. 1597-1614.
74. Zhang, H., et al., *Electrochemical lithium storage of titanate and titania nanotubes and nanorods*. Journal of Physical Chemistry C, 2007. **111**(16): p. 6143-6148.
75. Li, J., Z. Tang, and Z. Zhang, *Layered hydrogen titanate nanowires with novel lithium intercalation properties*. Chemistry of Materials, 2005. **17**(23): p. 5848-5855.
76. Li, J., Z. Tang, and Z. Zhang, *H-titanate nanotube: a novel lithium intercalation host with large capacity and high rate capability*. Electrochemistry Communications, 2005. **7**(1): p. 62-67.
77. Zhou, Y.K., et al., *Lithium Insertion into TiO<sub>2</sub> Nanotube Prepared by the Hydrothermal Process*. Journal of the Electrochemical Society, 2003. **150**(9): p. A1246-A1249.
78. Gao, X., et al., *Preparation and electrochemical characterization of anatase nanorods for lithium-inserting electrode material*. Journal of Physical Chemistry B, 2004. **108**(9): p. 2868-2872.
79. Li, J., Z. Tang, and Z. Zhang, *Pseudocapacitive characteristic of lithium ion storage in hydrogen titanate nanotubes*. Chemical Physics Letters, 2006. **418**(4-6): p. 506-510.
80. Wei, M., et al., *High rate performances of hydrogen titanate nanowires electrodes*. Electrochemistry Communications, 2008. **10**(8): p. 1164-1167.
81. Xu, J., et al., *Electrochemical properties of anatase TiO<sub>2</sub> nanotubes as an anode material for lithium-ion batteries*. Electrochimica Acta, 2007. **52**(28): p. 8044-8047.
82. Malik, M.A., M.Y. Wani, and M.A. Hashim, *Microemulsion method: A novel route to synthesize organic and inorganic nanomaterials: 1st Nano Update*. Arabian Journal of Chemistry, 2012. **5**(4): p. 397-417.
83. Yang, Q., et al., *Metal oxide and hydroxide nanoarrays: Hydrothermal synthesis and applications as supercapacitors and nanocatalysts*. Progress in Natural Science: Materials International, 2013. **23**(4): p. 351-366.
84. Su, C., B.Y. Hong, and C.M. Tseng, *Sol-gel preparation and photocatalysis of titanium dioxide*. Catalysis Today, 2004. **96**(3): p. 119-126.

85. Woo, K., et al., *Sol-Gel Mediated Synthesis of Fe<sub>2</sub>O<sub>3</sub> Nanorods*. *Advanced Materials*, 2003. **15**(20): p. 1761-1764.
86. Zhang, L. and H. Eckert, *Sol-gel synthesis of Al<sub>2</sub>O<sub>3</sub>-P<sub>2</sub>O<sub>5</sub> glasses: mechanistic studies by solution and solid state NMR*. *Journal of Materials Chemistry*, 2004. **14**(10): p. 1605-1615.
87. Sugimoto, T., X. Zhou, and A. Muramatsu, *Synthesis of uniform anatase TiO<sub>2</sub> nanoparticles by gel-sol method: 3. Formation process and size control*. *Journal of Colloid and Interface Science*, 2003. **259**(1): p. 43-52.
88. Brinker, C.J. and G.W. Scherer, *CHAPTER 1 - Introduction*, in *Sol-Gel Science*, C.J.B.W. Scherer, Editor. 1990, Academic Press: San Diego. p. xvi-18.
89. Sivakumar, S., et al., *Nanoporous titania-alumina mixed oxides—an alkoxide free sol-gel synthesis*. *Materials Letters*, 2004. **58**(21): p. 2664-2669.
90. Tonejc, A.M., I. Djerdj, and A. Tonejc, *Evidence from HRTEM image processing, XRD and EDS on nanocrystalline iron-doped titanium oxide powders*. *Materials Science and Engineering: B*, 2001. **85**(1): p. 55-63.
91. Yang, P., et al., *Titanium dioxide nanoparticles co-doped with Fe<sup>3+</sup> and Eu<sup>3+</sup> ions for photocatalysis*. *Materials Letters*, 2002. **57**(4): p. 794-801.
92. Wu, M., et al., *Sol-Hydrothermal Synthesis and Hydrothermally Structural Evolution of Nanocrystal Titanium Dioxide*. *Chemistry of Materials*, 2002. **14**(5): p. 1974-1980.
93. François, N., B. Ginzberg, and S. Bilmes, *Parameters Involved in the Sol-Gel Transition of Titania in Reverse Micelles*. *Journal of Sol-Gel Science and Technology*, 1998. **13**(1-3): p. 341-346.
94. Uekawa, N., et al., *Low Temperature Synthesis and Characterization of Porous Anatase TiO<sub>2</sub> Nanoparticles*. *Journal of Colloid and Interface Science*, 2002. **250**(2): p. 285-290.
95. Li, B., et al., *Preparation and characterization of nano-TiO<sub>2</sub> powder*. *Materials Chemistry and Physics*, 2003. **78**(1): p. 184-188.
96. Li, Y., T.J. White, and S.H. Lim, *Low-temperature synthesis and microstructural control of titania nano-particles*. *Journal of Solid State Chemistry*, 2004. **177**(4-5): p. 1372-1381.
97. Wong, C.L., Y.N. Tan, and A.R. Mohamed, *A review on the formation of titania nanotube photocatalysts by hydrothermal treatment*. *Journal of Environmental Management*, 2011. **92**(7): p. 1669-1680.
98. Lee, C.-K., et al., *Effects of sodium content and calcination temperature on the morphology, structure and photocatalytic activity of nanotubular titanates*. *Journal of Colloid and Interface Science*, 2007. **316**(2): p. 562-569.
99. Thorne, A., et al., *Formation, Structure, and Stability of Titanate Nanotubes and Their Proton Conductivity*. *J. Phys. Chem. B*, 2005. **109**(12): p. 5439-5444.
100. Yuan, Z.-Y. and B.-L. Su, *Titanium oxide nanotubes, nanofibers and nanowires*. *Colloids and Surfaces A: Physicochemical and Engineering Aspects*, 2004. **241**(1-3): p. 173-183.
101. Ou, H.-H. and S.-L. Lo, *Review of titania nanotubes synthesized via the hydrothermal treatment: Fabrication, modification, and application*. *Separation and Purification Technology*, 2007. **58**(1): p. 179-191.
102. Chen, Q., et al., *Trititanate Nanotubes Made via a Single Alkali Treatment*. *Advanced Materials*, 2002. **14**(17): p. 1208-1211.
103. Chen, Q., et al., *The structure of trititanate nanotubes*. *Acta Crystallogr B*, 2002. **58**(Pt 4): p. 587-93.
104. Sun, X. and Y. Li, *Synthesis and characterization of ion-exchangeable titanate nanotubes*. *Chem. - Eur. J.*, 2003. **9**(10): p. 2229-2238.
105. Yuan, Z.-Y. and B.-L. Su, *Titanium oxide nanotubes, nanofibers and nanowires*. *Colloids Surf., A*, 2004. **241**(1-3): p. 173-183.

106. Tian, Z.R., et al., *Large Oriented Arrays and Continuous Films of TiO<sub>2</sub>-Based Nanotubes*. Journal of the American Chemical Society, 2003. **125**(41): p. 12384-12385.
107. Ogawa, F., T. Ban, and Y. Ohya, *Preparation of lamellar hybrid inorganic–organic films of layered titanate and cationic or anionic surfactants*. Thin Solid Films, 2008. **516**(15): p. 4863-4867.
108. Hafizah, N. and I. Sopyan, *Nanosized TiO<sub>2</sub> Photocatalyst Powder via Sol-Gel Method: Effect of Hydrolysis Degree on Powder Properties*. International Journal of Photoenergy, 2009. **2009**: p. 8.
109. Subramanian, V., et al., *Nanocrystalline TiO<sub>2</sub> (anatase) for Li-ion batteries*. Journal of Power Sources, 2006. **159**(1): p. 186-192.
110. Zhang, H. and J.F. Banfield, *Understanding Polymorphic Phase Transformation Behavior during Growth of Nanocrystalline Aggregates: Insights from TiO<sub>2</sub>*. The Journal of Physical Chemistry B, 2000. **104**(15): p. 3481-3487.
111. Wang, C.-C. and J.Y. Ying, *Sol–Gel Synthesis and Hydrothermal Processing of Anatase and Rutile Titania Nanocrystals*. Chemistry of Materials, 1999. **11**(11): p. 3113-3120.
112. Ali Mehrizad, P.G. and S.M.T. , *Synthesis of nanosized TiO<sub>2</sub> powder by Sol-Gel method in acidic conditions* Journal of The Iranian Chemical Research, 2009. **2**: p. 145-149.
113. Shao, G.N., et al., *Sol–gel synthesis of photoactive zirconia–titania from metal salts and investigation of their photocatalytic properties in the photodegradation of methylene blue*. Powder Technology, 2014. **258**(0): p. 99-109.
114. Funda Sayilkan, Meltem Asilturk, and H. Sayilkan, *Characterization of TiO<sub>2</sub> Synthesized in Alcohol by a Sol-Gel Process: The Effects of Annealing Temperature and Acid Catalyst*. Turkish Journal of Chemistry, 2005. **29**.
115. van de Krol, R., A. Goossens, and E.A. Meulenkaamp, *In Situ X-Ray Diffraction of Lithium Intercalation in Nanostructured and Thin Film Anatase TiO<sub>2</sub>*. Journal of The Electrochemical Society, 1999. **146**(9): p. 3150-3154.
116. Krttil, P., et al., *Lithium insertion into self-organized mesoscopic TiO<sub>2</sub> (anatase) electrodes*. Solid State Ionics, 2000. **135**(1–4): p. 101-106.
117. Kavan, L., D. Fattakhova, and P. Krttil, *Lithium Insertion into Mesoscopic and Single-Crystal TiO<sub>2</sub> (Rutile) Electrodes*. Journal of The Electrochemical Society, 1999. **146**(4): p. 1375-1379.
118. Kavan, L., et al., *Nanocrystalline TiO<sub>2</sub> (anatase) electrodes: Surface morphology, adsorption, and electrochemical properties*. Journal of the Electrochemical Society, 1996. **143**(2): p. 394-400.
119. Wagemaker, M., A.P.M. Kentgens, and F.M. Mulder, *Equilibrium lithium transport between nanocrystalline phases in intercalated TiO<sub>2</sub> anatase*. Nature, 2002. **418**(6896): p. 397-399.
120. Jiang, C., et al., *Particle size dependence of the lithium storage capability and high rate performance of nanocrystalline anatase TiO<sub>2</sub> electrode*. Journal of Power Sources, 2007. **166**(1): p. 239-243.
121. Kavan, L., et al., *Surfactant-Templated TiO<sub>2</sub> (Anatase): Characteristic Features of Lithium Insertion Electrochemistry in Organized Nanostructures*. The Journal of Physical Chemistry B, 2000. **104**(50): p. 12012-12020.
122. Yang, J., et al., *Study on composition, structure and formation process of nanotube Na<sub>2</sub>Ti<sub>2</sub>O<sub>4</sub>(OH)<sub>2</sub>*. Dalton Trans., 2003(20): p. 3898-3901.
123. Tsai, C.-C. and H. Teng, *Regulation of the Physical Characteristics of Titania Nanotube Aggregates Synthesized from Hydrothermal Treatment*. Chem. Mater., 2004. **16**(22): p. 4352-4358.

124. Li, J., Z. Tang, and Z. Zhang, *Preparation and Novel Lithium Intercalation Properties of Titanium Oxide Nanotubes*. *Electrochemical and Solid-State Letters*, 2005. **8**(6): p. A316-A319.
125. Eom, M., et al., *Effect of Interlayer Spacing on the Electrochemical Properties of Alkali Titanate Nanotubes*. *Journal of Nanoscience and Nanotechnology*, 2013. **13**(5): p. 3742-3746.
126. Li, X., W. Liu, and J. Ni, *Short-cut synthesis of tri-titanate nanotubes using nano-anatase: Mechanism and application as an excellent adsorbent*. *Microporous and Mesoporous Materials*, 2015. **213**: p. 40-47.
127. Jausovec, D., et al., *Synergies of phenolic-acids' surface-modified titanate nanotubes (TiNT) for enhanced photo-catalytic activities*. *J Colloid Interface Sci*, 2015. **438**: p. 277-90.